Review

Organic Dyes for Light-Based Biomedical Imaging and Therapy

Panangattukara Prabhakaran Praveen Kumar *

Posted Date: 5 February 2026

doi: 10.20944/preprints202602.0438.v1

Keywords: organic dyes; diagnosis; imaging; photothermal therapy; photodynamic therapy; chemotherapy

 doi:10.20944/preprints202602.0438.v1

Review

Organic Dyes for Light-Based Biomedical Imaging and Therapy

Panangattukara Prabhakaran Praveen Kumar

Department of Biomedical Engineering and the Institute for Quantitative Health Science and Engineering, Michigan State University, East Lansing, MI 48824; p4praveen.18@gmail.com

Abstract

Light-based diagnostic and therapeutic approaches are increasingly important in modern biomedicine, with organic dyes emerging as versatile optical agents due to their tunable photophysical properties. Precise control over absorption and emission characteristics has enabled their application in fluorescence, photoacoustic, and Raman imaging, as well as in photodynamic and photothermal therapies. However, challenges related to biocompatibility, aqueous stability, and in vivo performance remain critical for clinical translation. Organic dyes that absorb in the near-infrared region are particularly attractive because of their deeper tissue penetration and reduced background interference. This review highlights key structure property relationships of organic dyes and summarizes current design strategies, including chromophore modification, peripheral functionalization for water solubility, and self-assembled nanotheranostic systems. Recent biomedical applications in cancer diagnosis and therapy, bacterial detection, and imaging-guided treatment are discussed, along with future directions for advancing dye-based technologies in healthcare.

Keywords: organic dyes; diagnosis; imaging; photothermal therapy; photodynamic therapy; chemotherapy

1. Introduction

Light-based technologies have emerged as powerful and versatile tools for probing biological systems and enabling non-invasive diagnosis and therapy across a wide range of diseases [1,2]. By complementing and extending conventional imaging and detection platforms, optical technologies have found broad applications in conditions such as inflammation, cancer, and cardiovascular disease. Among these approaches, fluorescence-based imaging has been extensively employed for molecular-level visualization due to its high sensitivity and specificity [3]. More recently, the integration of fluorescence imaging with photoacoustic imaging (PAI) has attracted significant attention. This hybrid modality combines strong optical contrast with ultrasound-based spatial resolution, enabling deeper tissue penetration and improved diagnostic accuracy, particularly for early disease detection in oncology [4,5].

Alongside diagnostic advancements, light-activated therapeutic modalities such as photothermal therapy (PTT) and photodynamic therapy (PDT) have gained prominence as minimally invasive cancer treatment strategies [6,7]. In these approaches, photoactive agents—commonly referred to as photosensitizers—convert absorbed light into localized heat (PTT) or generate cytotoxic reactive oxygen species, primarily singlet oxygen (PDT), resulting in targeted tumor ablation. Despite their therapeutic promise, achieving precise control over optical absorption, energy conversion pathways, and biological behavior remains a major challenge [8,9]. These limitations underscore the need for rationally designed materials with tunable optical properties, high photostability, and favorable biocompatibility.

Organic dyes represent a particularly attractive class of photoactive materials owing to their highly tunable molecular structures and diverse photophysical properties[10]. Since the discovery of

 doi:10.20944/preprints202602.0438.v1

the first synthetic azo dye (aniline yellow) in the nineteenth century, organic dyes have been widely utilized in fields ranging from textiles and solar energy conversion to optoelectronic devices such as light-emitting diodes[11,12]. In recent years, their role has expanded significantly into biomedical applications, driven by advances in molecular design and synthetic chemistry[13]. Dye families including cyanines, perylene and rylene derivatives, BODIPY dyes, indocyanine green, and aggregation-induced emission (AIE) luminogens have been extensively explored for bioimaging, photodynamic therapy, photothermal therapy, and, in some cases, image-guided chemotherapy [14,15].

A key advantage of organic dyes lies in the ability to precisely tailor their absorption and emission characteristics through chemical modification of the chromophore backbone and peripheral functional groups. Such modifications can induce pronounced spectral shifts, modulate fluorescence intensity, or alter non-radiative decay pathways. While some colorimetric changes are visible to the naked eye, most biological applications rely on fluorescence- or photoacoustic-based signal modulation for sensitive in vitro and in vivo detection. Organic dyes absorbing in the near-infrared (NIR-I and NIR-II) spectral windows enable deeper tissue penetration, reduced autofluorescence, and improved signal-to-noise ratios, making them highly suitable for biomedical imaging[16,17].

Beyond fluorescence, organic dyes can also be engineered to favor non-radiative relaxation processes, efficiently converting absorbed optical energy into heat. This property is especially advantageous for photoacoustic imaging, where transient thermoelastic expansion generates detectable acoustic waves with high spatial resolution [16,18]. Dye-based photoacoustic probes have therefore enabled non-invasive visualization of tumors, inflammatory lesions, and vascular abnormalities, addressing several limitations associated with conventional diagnostic techniques[19,20].

Despite these advantages, the clinical translation of organic dyes is often hindered by poor aqueous solubility and limited stability in biological environments. Significant progress has been made to address these challenges through chemical functionalization with hydrophilic moieties, polymer conjugation, and supramolecular assembly [21,22]. Furthermore, advances in nanomaterial synthesis and nanoprecipitation strategies have enabled organic dyes to be encapsulated within or conjugated to inorganic and hybrid nanostructures [23,24]. These nanoformulations enhance water solubility, photostability, circulation time, and targeting capability. For example, BODIPY dyes functionalized with hydrophilic groups or integrated with inorganic nanoparticles such as gold nanostructures exhibit improved performance in bioimaging, photodynamic therapy, and photothermal therapy due to synergistic optical and photothermal effects[14].

This review highlights recent advances in the design and biomedical application of organic dyes and their nanoformulations, with a particular emphasis on imaging, phototherapy, and emerging theranostic strategies. Special attention is given to structure–property relationships, optical tuning approaches, and translational challenges relevant to the development of next-generation light-based diagnostic and therapeutic platforms.

2. Design Strategy

The design of organic dyes is highly application-dependent, with molecular architecture playing a central role in determining their optical behavior. Incorporation of diverse donor–acceptor motifs within the conjugated backbone enables precise modulation of photophysical properties, allowing absorption profiles to be shifted toward the far-red and near-infrared regions [25,26]. To enhance aqueous compatibility, dyes can be functionalized with hydrophilic moieties or transformed into nanoformulations using strategies such as nanoprecipitation, self-assembly, or supramolecular interactions[27]. Representative organic dyes commonly employed in biomedical applications are illustrated in Figure 1A.

 doi:10.20944/preprints202602.0438.v1

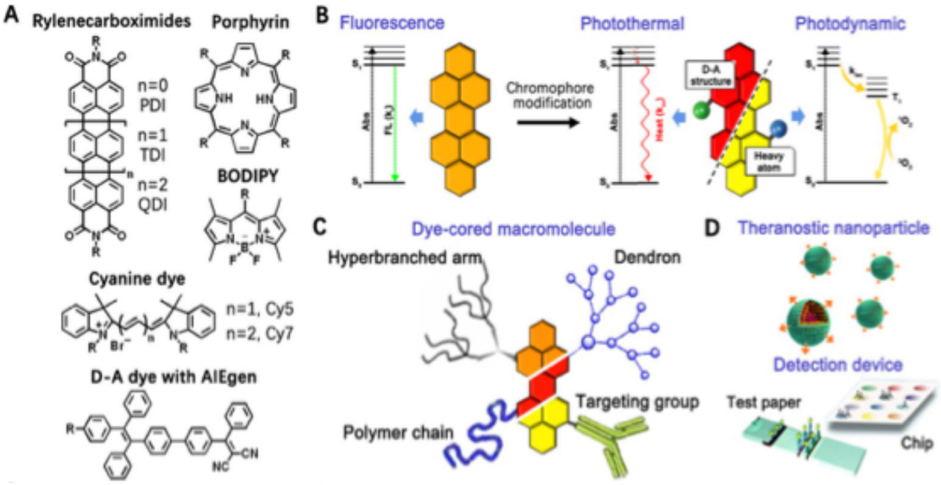

Figure 1. (A) Representative chemical structures of selected organic dyes used in biomedical applications. (B) Modulation of dye photophysical pathways—fluorescence emission, photothermal conversion, and photodynamic activity—through molecular design. Abs denote absorbance, k_{nr} the nonradiative decay rate, and k_{ISC} the intersystem crossing rate. (C) Schematic illustration of a functionalized dye-cored macromolecular architecture. (D) Overview of functional organic dye–based material platforms for imaging and therapeutic applications. Reproduced under the terms and conditions of Creative Commons Attribution 4.0 International (CC BY) license [13]. Copyright 2020.

Upon excitation at appropriate wavelengths, organic dyes can undergo radiative emission, non-radiative heat dissipation, or generate reactive oxygen species, depending on their molecular structure. These photophysical pathways can be finely regulated through chemical modification of the dye backbone (Figure 1B). Fluorophores such as BODIPY, cyanine, and perylene derivatives exhibit strong fluorescence and are widely utilized in bioimaging [14,15]. Structural engineering of these dyes further enables their application in light-activated therapeutic modalities. For example, the introduction of heavy atoms such as bromine or iodine promotes intersystem crossing, thereby modulating fluorescence quantum yield and enhancing photothermal or photodynamic efficiency (Figure 1B) [28,29]. Dyes with inherently low fluorescence quantum yields preferentially convert absorbed light into heat, making them particularly suitable for photoacoustic imaging as well as photothermal and photodynamic therapies [30].

Despite their favorable optical properties, many organic dyes possess hydrophobic cores that limit their direct use in biological environments due to aggregation in aqueous or physiological media. This limitation can be addressed by incorporating hydrophilic functional groups such as polyethylene glycol chains, glycol or ether linkages, or charged moieties including amines, carboxylates, phosphates, and sulfonates (Figure 1C)[15]. Recent studies have demonstrated that core–shell macromolecular dye architectures bearing hydrophilic outer layers significantly improve aqueous stability while preserving optical performance [31]. Such designs have shown promise in bioimaging, drug delivery, and tumor-targeted therapeutic applications by reducing aggregation and enhancing circulation stability (Figure 1C).

Leveraging their distinctive optical characteristics and surface chemistry, organic dyes have increasingly been engineered into nanoscale materials for energy and biomedical applications. Dye-based nanoparticles can be prepared through nanoprecipitation or by encapsulation within polymeric or metallic nanocarriers[32]. Owing to their rigid and planar molecular structures, organic dyes readily assemble through π–π stacking and hydrophobic interactions, enabling the formation of nanoscale imaging agents and nanomedicines. Like inorganic nanomaterials, organic dye assemblies can achieve ultrasmall particle sizes depending on the extent of molecular aggregation[23]. These nanostructures can serve as carriers for hydrophobic therapeutics, with light-triggered release at target sites. Additionally, incorporation of dyes into metal–organic frameworks

 doi:10.20944/preprints202602.0438.v1

or hydrogel matrices has emerged as an effective approach for controlled drug delivery and photothermal-based therapeutic interventions.

Organic dyes also play an important role in in vitro analytical and diagnostic applications. By incorporating stimulus-responsive functional groups into fluorescent dye structures, highly selective probes can be engineered for the detection of gases, metal ions, disease-associated biomarkers, and antibodies[33]. These fluorescent sensing platforms range from simple formats, such as polymer-based fluorescent films and paper-based test strips, to more advanced systems, including fluorescent microarrays and chip-based sensors designed for microscopic analysis (Figure 1 D) [34]. In such systems, overall sensing performance is strongly influenced not only by the intrinsic photophysical properties of the dye but also by its interaction with the supporting substrate and the strategy used to immobilize or couple the probe to the sensing platform.

3. Healthcare Applications

3.1. Antimicrobial and Antibacterial Applications

Bacterial infection remains one of the major concerns in public health[35]. Antimicrobial agents are widely used to kill microorganisms and suppress their growth, and recent developments have introduced a variety of synthetic and natural antimicrobial agents. Identifying pathogens such as bacteria is a crucial first step, followed by their disinfection using appropriate antimicrobial agents. Advances in fluorescence and chemiluminescence based on organic dyes have led to the development of antimicrobial systems that enable facile pathogen detection[36]. These systems exploit surface functionalities that interact with bacterial components to generate detectable fluorescence signals. Although growth inhibition tests remain the gold standard, technological advancements have introduced simpler detection approaches, including colorimetric assays and paper-based test strips [37].

Boehle et al. prepared a paper test strip for β-lactamase-mediated resistance detection using nitrocefin [38]. Cleavage of nitrocefin by β-lactamase produced a visible color change from yellow to red, as shown in Figure 2A. The β-lactamase–nitrocefin reaction was optimized in phosphate-buffered saline at pH 7.5, with an optimal nitrocefin concentration of 0.5 mM, achieving a detection limit of 10 mU/mL for lyophilized enzyme. Under these optimized conditions, β-lactamase activity was detected directly in live E. coli without culturing. A visible color change was observed only in β-lactamase-expressing bacteria, with a detection threshold above 3.8×10^6 CFU/mL (Figure 2B). Importantly, non-β-lactamase-producing bacteria did not interfere with signal generation, as comparable color intensities were observed in both pure and mixed bacterial populations. Cell lysis resulted in only a modest enhancement in assay performance, with an approximately 5% increase in signal intensity after 10 min compared to intact cells. This minimal improvement suggests that β-lactamase is either released from bacterial cells or that nitrocefin readily penetrates the bacterial membrane, enabling effective detection without additional sample processing.

Aggregation-induced emission (AIE) luminogen-based dyes and nanoparticles have also found applications in bacterial detection through fluorescence-based approaches. Chen et al. developed an antimicrobial polymer incorporating ester linkages between the polymer backbone and functional units, while integrating AIE luminogens to enable simultaneous bacterial imaging and eradication (Figure 2C) [39]. The cationic segments of the polymer electrostatically interact with negatively charged bacterial membranes, while hydrophobic alkyl chains insert into the lipid bilayer, collectively disrupting membrane integrity. The ester bonds impart strong short-term antibacterial activity and undergo enzymatic hydrolysis in biological environments, thereby improving biocompatibility. The resulting Q-PGEDA-OP/TPE system achieved antibacterial efficiencies exceeding 99% against both S. aureus and E. coli, with SEM analysis confirming severe membrane damage (Figure 2C). Similarly, Wang et al. demonstrated that AIEgen-based nanostructures can function as both photodynamic and photothermal antibacterial agents, achieving antibacterial rates as high as 99.9% for S. aureus and 99.8% for E. coli [40].

 doi:10.20944/preprints202602.0438.v1

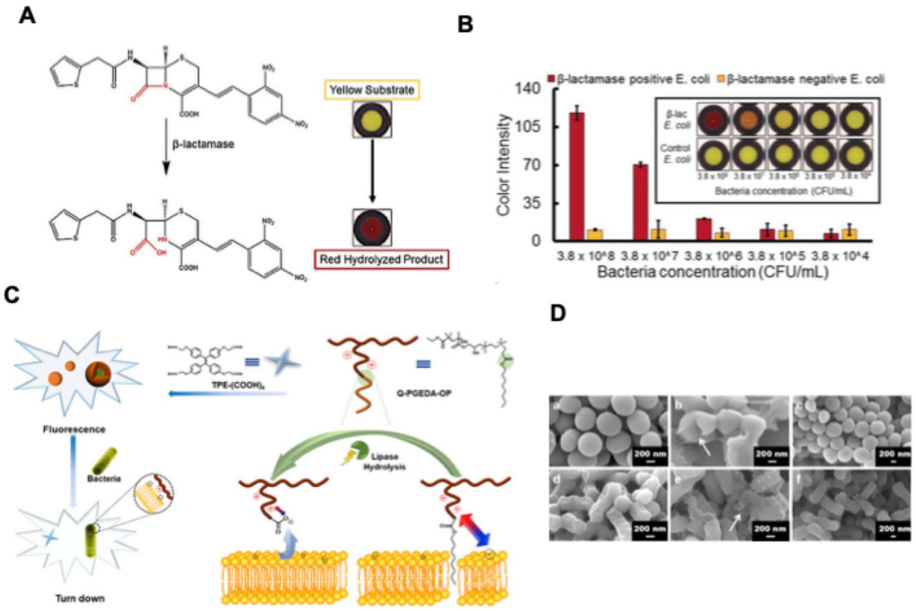

Figure 2. (A) Schematic representation of the enzymatic interaction between β-lactamase and nitrocefin. Cleavage of the β-lactam ring in nitrocefin by β-lactamase induces a pronounced chromatic transition from yellow to red, enabling rapid and visually interpretable detection. (B) Performance evaluation of the paper-based assay using serial dilutions of bacterial samples with and without β-lactamase expression, highlighting the assay's specificity and discriminatory capability. Reproduced with permission from[38], Copyright 2017, Wiley Publishers. C) Schematic representation of the design and modulation of the well-defined polymeric Q-PGEDA-OP/TPE antimicrobial platform, illustrating its application in bacterial sensing and antibacterial performance before and after hydrolytic transformation. (D) SEM micrographs of AMO-treated S. aureus (a–c) and E. coli (d–f) following exposure to PBS (a,d), Q-PGEDA-OP (b,e), and the hydrolyzed form Q-PGEDA-COOH (c,f). Scale bars correspond to 200 nm. Reproduced with permission from [39], Copyright 2018, American Chemical Society.

Perylene diimides (PDI) possess excellent fluorescence and photothermal properties. Conjugation of the perylene core with water-soluble groups has enabled the fabrication of a series of fluorescent dyes for biomedical applications [15]. Yang et al. reported a supramolecular complex formed between cucurbit [7]uril and perylene diimides [41]. Facultative anaerobic bacteria such as E. coli exhibit sufficient reducing activity to generate radical anions of the dye complex in situ, enabling effective photothermal killing under near-infrared irradiation. In contrast, aerobic bacteria such as B. subtilis lack the reductive capacity required for dye complex activation and therefore do not generate photothermally active species. This differential redox response enables the dye complex to selectively inhibit specific bacterial populations through photothermal therapy.

3.2. Disease Diagnosis

3.2.1. In Vitro Diagnosis

Detection of biomarkers and biomolecules is essential because their analysis provides valuable information about disease progression and treatment monitoring[42,43]. Among various diagnostic tools, organic dyes have gained wide attention due to their good biocompatibility and strong optical properties, offering advantages over many inorganic materials. Traditional techniques such as chromatography, electrophoresis, and electrochemical methods are often time-consuming and less suitable for rapid or early diagnosis[44]. In contrast, recent advances in fluorescent and chemiluminescent organic materials have made biomarker detection faster, simpler, and more accessible[33].

 doi:10.20944/preprints202602.0438.v1

Ai and Lu et al. developed imidazolium-functionalized polydiacetylenes (iPDAs) as a sensing system for the rapid and selective detection of lysobisphosphatidic acid (LPA), a biomarker linked to early-stage ovarian cancer (Figure 3A) [45]. This system operates through a "lock–key" mechanism, where LPA interacts specifically with the iPDA structure via electrostatic and hydrophobic interactions. Upon binding, the iPDA backbone undergoes a structural change, producing a visible color shift from blue to red. This color change enables quantitative detection of LPA in plasma (Figure 3B). Using this approach, the authors further developed a portable point-of-care device capable of reliably distinguishing blood samples from ovarian cancer patients and healthy individuals (Figure 3C).

In parallel, microarray-on-chip technologies have emerged as powerful tools for rapid and multiplexed biomarker detection. Hucknall et al. introduced an inkjet-printed microarray platform, known as the D4 assay chip, designed for quantitative and self-contained immunoassays [46]. By correlating fluorescence intensity with analyte concentration in IL-6-spiked serum samples, accurate quantification of IL-6 was achieved. Additionally, multiple biomarkers could be detected simultaneously by printing different capture spots on a single chip. Compared with conventional ELISA methods, the D4 assay is faster, easier to use, and well suited for rapid blood-based diagnostics and early disease detection.

Water soluble PDIs are widely used for in vitro cellular imaging owing to their intrinsic fluorescence which is highly sensitive to various stimuli such as temperature and pH of media which allow visualization of cellular structure and cellular process. Zimmerman and co-workers developed a polyglycerol-dendronized perylene diimide, functionalized with a single biotin moiety for targeted fluorescence imaging applications (Figure 3D) [47]. Upon attachment to PEG-passivated substrates through biotin–neutravidin interactions, the fluorophore displayed strong and selective fluorescence, demonstrating its targeting specificity. In live E. coli cells expressing biotinylated surface receptors, prior treatment with streptavidin resulted in distinct fluorescent localization on the bacterial membrane, occasionally appearing as helical patterns that reflect underlying protein organization. These results demonstrate the utility of perlyene as a high-precision fluorescent probe and introduce a versatile biolabeling concept that combines a fluorescent core with a multivalent dendritic shell for targeted imaging and potential therapeutic use (Figure 3E). In a related study, a guanidinium-functionalized dendronized perylene analogue was shown to efficiently enter HeLa cells and accumulate within the cytoplasm, enabling effective intracellular fluorescence imaging [48].

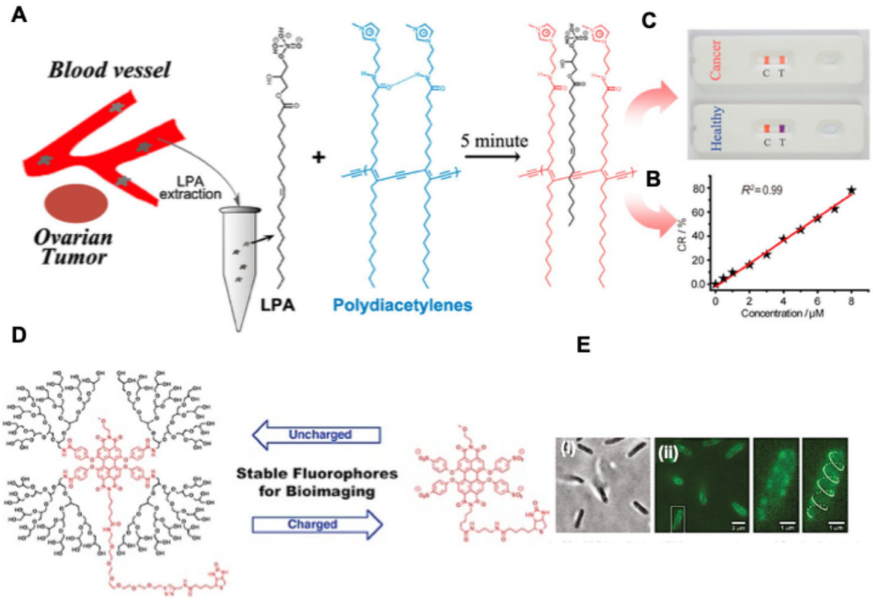

Figure 3. (A) Schematic illustration of the sensing mechanism employed for lysophosphatidic acid (LPA) recognition. (B) Colorimetric response of iPDAs as a function of increasing LPA molar equivalents. (C)

 doi:10.20944/preprints202602.0438.v1

Conceptual depiction of an LPA-driven point-of-care diagnostic strategy for ovarian cancer detection. Reproduced with permission from [45]. Copyright 2017 American Chemical Society. (D) (D) Molecular structure of polyglycerol-dendronized perylene diimide. (B) Bright-field (i, ii) and fluorescence microscopy images of E. coli following labeling with PDI-41 after streptavidin preincubation. The enlarged panel on the right corresponds to the boxed region in the central image, highlighting the helical distribution of λ receptors within an individual bacterium. Reproduced with permission from [47]. Copyright 2011, American Chemical Society.

BODIPY dyes have been extensively used for various in vitro bioimaging applications[14]. They have been used for cell membrane imaging, mitochondria, cytosol, and for endoplasmic reticulum imaging with proper surface modifications and charges [49]. To enhance plasma membrane–specific bioimaging, Collot et al. developed BODIPY-based plasma membrane probes by introducing amphiphilic and zwitterionic anchors to a green-emitting BODIPY core, generating variants with one to three anchors [50]. Among them, only oneprobe exhibited the best performance, showing a high quantum yield (0.92) and superior membrane specificity. Unlike conventional membrane labels such as fluorescent lectins, this probe remains non-emissive in aqueous environments and becomes strongly fluorescent only upon membrane binding, resulting in significantly higher signal-to-noise ratios. Across multiple cell models, including KB, HeLa, and U87 spheroids, the probe enabled bright, membrane-specific imaging using confocal and two-photon microscopy, with minimal cytotoxicity and favorable biodistribution, highlighting its advantages over traditional membrane-staining agents.

Recent studies demonstrate how structural modification of BODIPY probes enables distinct membrane-focused imaging and therapeutic functions. Polita et al. reported a viscosity-responsive s-indacene BODIPY probe that rapidly stains plasma membranes and enables fluorescence-lifetime-based mapping of membrane and cytoplasmic viscosity in live A549 cells[51]. In contrast, Li et al. introduced a fluorinated aza-BODIPY platform that combines fluorescence imaging with ^{19}F MRI, enabling simultaneous membrane visualization, oxygen mapping, and photodynamic therapy guidance [52]. Fluorination enhanced membrane affinity and photosensitization, leading to singlet-oxygen-mediated lipid oxidation and pyroptosis, effectively suppressing tumor growth in vivo.

Complementing these approaches, Xiong et al. developed a pyrazolone-functionalized BODIPY probe designed for long-term plasma membrane imaging. Unlike internalizing probes, this derivative binds noncovalently to membrane proteins and remains membrane-confined, providing stable, photobleaching-resistant fluorescence for over 96 h [53]. Collectively, these studies illustrate how viscosity sensitivity, fluorination, and functional anchoring endow BODIPY probes with complementary capabilities ranging from biophysical sensing to image-guided therapy.

Recent advances in BODIPY probe design demonstrate how targeted structural modifications enable control over solubility, spectral tuning, and cellular localization for bioimaging applications. Alkene substitution combined with ester or carboxylic acid groups effectively shifts BODIPY absorption and emission into the far-red and near-infrared regions (≈627–747 nm) while improving aqueous solubility and fluorescence efficiency, enabling sensitive imaging of cancer cells with high contrast [54]. Extension of π-conjugation through rigid chromophoric units further enhances NIR emission and induces turn-on fluorescence responses upon cellular interaction, supporting deep-tissue imaging and potential photodynamic applications with low cytotoxicity [55]. In parallel, sulfonation strategies provide precise control over cellular permeability and probe localization, where mono-sulfonated BODIPYs readily cross cell membranes and di-sulfonated analogues remain confined to cell-surface receptors [56]. Collectively, these approaches highlight complementary design principles—spectral red-shifting via conjugation and alkene substitution, solubility enhancement through polar functionalities, and localization control via ionic groups—underscoring the versatility of BODIPY platforms for tailored intracellular and surface-targeted bioimaging, while also emphasizing the need for systematic in vivo validation to fully establish translational potential.

 doi:10.20944/preprints202602.0438.v1

3.2.2. In Vivo Diagnosis

Photoacoustic and fluorescence-based imaging is the commonly used two methods for the in vivo diagnosis of various diseases especially for tumors using organic dyes[57,58]. The dyes with NIR absorption in region I and II can be exclusively used for such imaging applications due to deep tissue penetration capability and reduced noise from backgrounds. Such non-invasive based imaging platforms are widely used these days for in vivo imaging and early detection of various biomarkers with short exposure time.

Urano et al fabricated a fluorescent probe HMRef-βGal based on optimized spirocyclization strategy for in vivo visualizing peritoneal metastatic tumors [59]. This membrane permeable dye showed enhanced fluorescence turn on upto 1,400-fold fluorescence enhancement on activation. After confirming its ability to detect intracellular β-galactosidase activity, HMRef-βGal was evaluated for in vivo cancer imaging using a mouse model of peritoneal metastasis. Following intraperitoneal administration, HMRef-βGal enabled rapid and specific visualization of metastatic nodules smaller than 1 mm, with fluorescence intensity increasing over time to allow clear identification of tumors, including by naked eye observation. The detected lesions were confirmed as ovarian cancer metastases through colocalization with a lectin-based stain, and signal suppression by a β-galactosidase inhibitor verified enzyme-specific activation. Importantly, HMRef-βGal successfully visualized peritoneal metastases across multiple ovarian cancer models, including cell lines that were not detectable using earlier enzyme-targeted probes, highlighting its broad applicability for metastatic cancer imaging.

BODIPY [14], Aza-bodipy [49], and perlyene derivatives [15], indocyano green [60], cyanines [61]etc. were widely employed for in vivo tumor imaging applications. For in vivo imaging applications, the organic dyes were mostly converted into their nano formulations for improved biocompatibility and blood circulation. Perylene diimide–based nanoparticles (PDI NPs) have gained increasing attention as robust fluorescent probes for bioimaging due to their excellent photostability and tunable optical properties [62]. NIR and emerging NIR-II PDI systems enable deep-tissue imaging with reduced background interference, supporting applications in high-resolution cancer diagnosis and therapy monitoring. Zong et al. reported PDI NPs engineered with a carbazole-based isolation unit to regulate dye aggregation (Figure 4A) [63]. These nanoparticles, fabricated via nanoprecipitation using Pluronic F-127, exhibited strong deep-red emission (λ_max = 658 nm), high photostability (≈79% signal retention after prolonged laser irradiation), and an average hydrodynamic diameter of ~100 nm (Figure 4B–D). When combined with three-photon excitation microscopy, PDI NPs enabled high-contrast imaging of mouse cerebral vasculature through the intact skull, achieving penetration depths up to 450 μm (Figure 4E).

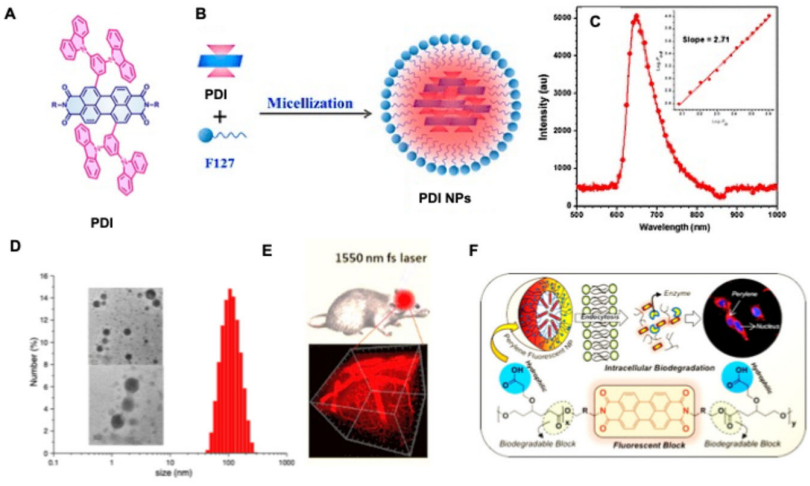

Figure 4. (A) Molecular structure of carbazole-PDI derivative. (B) Self-assembly of carbazole-PDI into nanoparticles via micelle formation using Pluronic F127. (C) Photoluminescence emission spectra of carbazole-

 doi:10.20944/preprints202602.0438.v1

PDI NPs following laser irradiation. (D) Morphological and size characterization of carbazole-PDI NPs determined by TEM imaging and DLS analysis. (E) Three-dimensional reconstructed image illustrating the vascular distribution of carbazole-PDI NPs in a mouse model (scale bar: 100 μm). Reproduced with permission from [63]. Copyright 2018, American Chemical Society. (F) Schematic illustration of the design and synthesis of PDI-functionalized amphiphilic PCL block copolymers, their nanoassembly into PDI NPs, and their application in intracellular enzyme-responsive bioimaging. Reproduced with permission from [64]. Copyright 2019, American Chemical Society.

In a complementary strategy, a biodegradable and enzyme-responsive polycaprolactone (CPCL]-based PDI nanoprobe was developed for intracellular imaging (Figure 4F) [64]. Amphiphilic PDI-CPCL block copolymers self-assembled into stable spherical nanoparticles (~100 nm) in aqueous media and exhibited suitable fluorescence efficiencies (Φ = 0.25–0.30). These nanoprobes demonstrated excellent biocompatibility and efficient cellular uptake via endocytosis, with preferential accumulation in the perinuclear region of both normal and cancer cells, highlighting their potential for intracellular fluorescence imaging.

BODIPY/aza-BODIPY dyes can be used for multimodal imaging applications owing to labile and exchangeable groups in their backbone. Early work by Li and co-workers in 2011 established the feasibility of BODIPY dyes as dual positron emission tomography (PET) and fluorescence imaging agents through the successful radiofluorination of a hydroxyl-functionalized BODIPY using an [^{18}F]TBAF complex [65]. Following systemic administration of the resulting [^{18}F]BODIPY probe in mice, in vivo PET imaging revealed predominant accumulation in the kidneys and liver, with no detectable bone uptake, indicating favorable in vivo stability of the C–^{18}F bond. Additional uptake in the gall bladder suggested hepatobiliary clearance. Importantly, ex vivo fluorescence and PET analyses showed consistent organ distribution profiles, confirming the reliability of the probe for multimodal imaging. Building on this concept, Chansaenpak and co-workers systematically investigated a series of cationic ammonium-substituted [^{18}F]BODIPY derivatives to assess their suitability as PET imaging probes [66]. By varying the nitrogen substituents at the meso position, they identified a BODIPY derivative bearing two methyl groups and one ethyl group on the ammonium center as particularly promising, exhibiting low lipophilicity (log P = 1.04), pronounced cardiac uptake, and favorable heart-to-organ contrast ratios. To introduce tumor specificity, BODIPY probes were further functionalized with targeting ligands such as the Arg–Gly–Asp (RGD) peptide, which binds selectively to integrin $\alpha v\beta 3$ overexpressed in glioblastoma cells. In vivo and ex vivo imaging studies using an RGD-conjugated [^{18}F]BODIPY probe in U87MG tumor–bearing mice demonstrated strong tumor uptake in both PET and fluorescence modalities [67]. While PET imaging revealed tracer accumulation in the liver, kidneys, and tumor, fluorescence imaging provided enhanced tumor contrast due to reduced hemoglobin-mediated optical absorption in the less vascularized tumor tissue. This complementary behavior highlights the advantage of combining nuclear and optical readouts. Consistent results were further obtained using a dimeric RGD-conjugated BODIPY probe , which exhibited high tumor accumulation in both PET and fluorescence images at 2 h post-injection in glioblastoma xenograft models[68]. Collectively, these studies demonstrate the versatility and reliability of [^{18}F]BODIPY-based platforms for dual-modality imaging and targeted cancer visualization.

Indocyanine green (ICG) is an FDA approved NIR dye used for various bioimaging and light-based therapy[60]. Even though its FDA approved, the solubility, photostability, biocompatibility etc. is a threat for their smooth use. Many nanoformulations have developed in which ICG is conjugated to proteins, polymers, peptides etc. for smooth delivery and stability for future biomedical applications. Owing to the strong fluorescence in the NIR region, ICG is used for visualization of tumors, and inflammations using fluorescence microscopy. ICG–based fluorescence imaging has emerged as a promising approach for intraoperative tumor visualization and margin assessment in breast-conserving surgery. In a clinical study involving 40 patients, ICG fluorescence images acquired at multiple surgical stages—including in situ tumors, post-excision cavities, freshly excised

 doi:10.20944/preprints202602.0438.v1

specimens, and histopathology grossing—were analyzed using intensity- and texture-based imaging features [69]. Machine-learning models, including logistic regression and support vector machines, demonstrated that combining fluorescence intensity with spatial texture metrics improved tumor extent prediction with pixel-level resolution. Notably, ICG fluorescence was preserved following formalin fixation, enabling validation of imaging findings across fresh and fixed tissue samples. The trained models achieved high sensitivity and specificity in identifying tumor regions and were successfully extended to predict residual disease in surgical cavities. Collectively, these findings highlight the potential of quantitative ICG fluorescence imaging, coupled with data-driven analysis, as a practical tool for real-time intraoperative decision-making and post-excision tumor assessment. Chen et al used ICG dye for targeted prostate cancer, by conjugating ICG to prostate-specific membrane antigen targeting peptide (PSMA) [70]. In vivo studies showed tumor targeting specificity and identification of the probe under fluorescence microscope enabled surgical guidance for the tumor resection. This work further extended for human patient having prostate cancer. A 62-year-old male patient (67 kg) with biopsy-confirmed prostate cancer presented with markedly elevated prostate-specific antigen levels (total PSA: 21 ng/mL). Preoperative staging using positron emission tomography/computed tomography and magnetic resonance imaging revealed no evidence of distant metastasis, consistent with a localized primary malignancy. Fluorescence-guided laparoscopic radical prostatectomy was performed using an endoscopic imaging platform. The patient received a single intravenous dose of the PSMA-targeted probe ICG-PSMA-D5 (0.03 mg/kg) 24 h prior to surgery. The procedure was well tolerated, with no observable adverse events or clinically significant pharmacological effects. Albumin-ICG nanoparticles are used for a wide variety of tumor imaging and therapy applications [71,72]. Due to the large circulation time, biocompatibility of albumin nanoparticles, ICG conjugated such nanoparticles were used endometriosis detection, and for inflammation studies.

4. Photoacoustic Imaging Applications

Photoacoustic imaging (PAI) has emerged as a powerful biomedical imaging modality by combining the high contrast of optical excitation with the deep tissue penetration of ultrasound detection [20,73]. A wide range of photoacoustic contrast agents, including inorganic nanomaterials and organic dyes, have been developed to enhance imaging performance[18]. Among these, small-molecule probes are particularly attractive for translational applications due to their favorable in vivo behavior and ease of chemical modification. Recent advances in near-infrared (700–1700 nm) PAI have further improved imaging depth and quality by minimizing optical scattering compared to visible wavelengths, enabling more effective visualization of deep biological tissues [74]. In 2008 wang et al. reported first time use of ICG for PAI for brain tumors in vivo [75]. This study opens new pathway for the use of organic dyes for PAI applications.

Studies have shown that incorporating PEG to ICG formulations can improve their solubility and increase the PA signal intensity due to the strong absorption coefficient of ICG after assembly. In 2017, Saji and co-workers improved the aqueous compatibility and photoacoustic performance of ICG by conjugating it with polysarcosine, leading to the formation of stable nanoparticles that enhanced photoacoustic signal intensity[76]. This ICG–polysarcosine nanosystem exhibited rapid tumor accumulation in vivo, which was attributed to the favorable transport and tumor-penetrating characteristics of the polymer, thereby improving probe localization within tumor tissue. Subsequently, Poggi et al. developed an integrin-targeted photoacoustic probe by coupling ICG to an RGD peptide [77]. In vivo photoacoustic imaging demonstrated that ligand-based functionalization not only improved ICG solubility but also prolonged its retention within tumor regions, underscoring the value of molecular targeting strategies for enhancing tumor-specific photoacoustic contrast.

Ratiometric photoacoustic (PA) probes have been developed to improve in vivo signal-to-noise ratios by enabling self-referenced detection of endogenous biomarkers, thereby minimizing interference from tissue heterogeneity and physiological fluctuations. By generating two spectrally distinct PA signals—one responsive and one invariant—these probes provide intrinsic calibration

 doi:10.20944/preprints202602.0438.v1

and more reliable quantification in complex biological environments [78]. Chen et al. introduced a Cu^{2+}-responsive ratiometric PA system by co-encapsulating a copper-sensitive dye and a nonresponsive reference dye within nanomicelles, achieving selective and quantitative Cu^{2+} detection through wavelength-dependent PA signal changes [79]. Similarly, Fan et al. designed a small-molecule cyanine-based probe capable of ratiometric hydrogen sulfide sensing, where nucleophilic reaction with H_2S produced opposite PA responses at two wavelengths, enabling sensitive detection at physiological concentrations and successful in vivo imaging with rapid probe clearance [80].

Beyond ratiometric strategies, molecular engineering has been widely employed to enhance PA performance by shifting absorption into the near-infrared region and promoting nonradiative energy dissipation. Squaraine dyes, which undergo aggregation-induced red shifts in aqueous environments, were adapted for PA imaging through albumin-assisted stabilization, enabling effective NIR signal generation [81,82]. Structural modification of BODIPY dyes through conjugation with electron-rich moieties, such as 1H-pyrrole, has also been shown to induce red-shifted absorption and fluorescence quenching via photoinduced electron transfer, thereby enhancing PA output [83]. In parallel, metal–ligand coordination has emerged as an effective approach to strengthen push–pull electronic interactions, as demonstrated by iron(II) complexes with high photothermal conversion efficiency and strong PA signals combined with favorable biocompatibility [84].

Fundamental photophysical studies further revealed that enhanced PA emission in organic dyes is closely linked to efficient excited-state absorption and rapid nonradiative relaxation pathways. Comparative investigations of BODIPY, cyanine, and curcumin-based systems showed that tailored donor–π–acceptor architectures significantly amplify PA signals, with nonlinear increases observed at higher excitation fluence. These insights provide a mechanistic foundation for the rational design of next-generation PA contrast agents with improved sensitivity and imaging depth.

Naphthalocyanine -based nanoformulations have been extensively explored as high-performance contrast agents for photoacoustic imaging (PAI) and image-guided therapy[85,86]. Zhang and co-workers developed a series of nanoformulated naphthalocyanine dyes with tunable absorption profiles for in vivo PAI of the gastrointestinal tract and lymphatic system (Figure 5A-B)[87,88]. By adjusting the dye structure, they generated multicolor probes that enabled clear visualization of lymphatic networks and facilitated multispectral imaging, in which distinct tracers with different near-infrared absorption maxima were used to independently map bilateral lymphatic drainage pathways (Figure 5C). Building on these imaging capabilities, the same group later optimized naphthalocyanine nanoformulations for theranostic applications in 4T1 breast cancer models by increasing dye loading through removal of excess surfactant [89]. The resulting nanoparticles exhibited strong near-infrared absorption, enabling both tumor-specific photoacoustic contrast and effective photothermal therapy. Complementary work by Choi et al. introduced naphthalocyanine-loaded nanodroplets designed for high-intensity focused ultrasound (HIFU)–guided tumor ablation (Figure 5D) [90]. Encapsulation of the dye within a perfluorohexane core produced agents with pronounced absorption in the near-infrared region (Figure 5E) and robust in vivo imaging performance following systemic administration in breast tumor–bearing mice (Figure 5F). In addition to providing photoacoustic contrast, these nanodroplets enabled efficient HIFU-mediated tumor destruction, as confirmed by post-treatment tumor regression measurements.

PDI–based materials have attracted growing interest as photoacoustic (PA) contrast agents due to their strong optical absorption, high photostability, and efficient nonradiative energy conversion. These intrinsic properties enable effective transformation of absorbed light into acoustic signals, making PDI nanostructures particularly suitable for high-resolution imaging of deep tissues. Recent studies have demonstrated that rational molecular design and nanoparticle formulation can further optimize PDI systems for in vivo photoacoustic applications.

 doi:10.20944/preprints202602.0438.v1

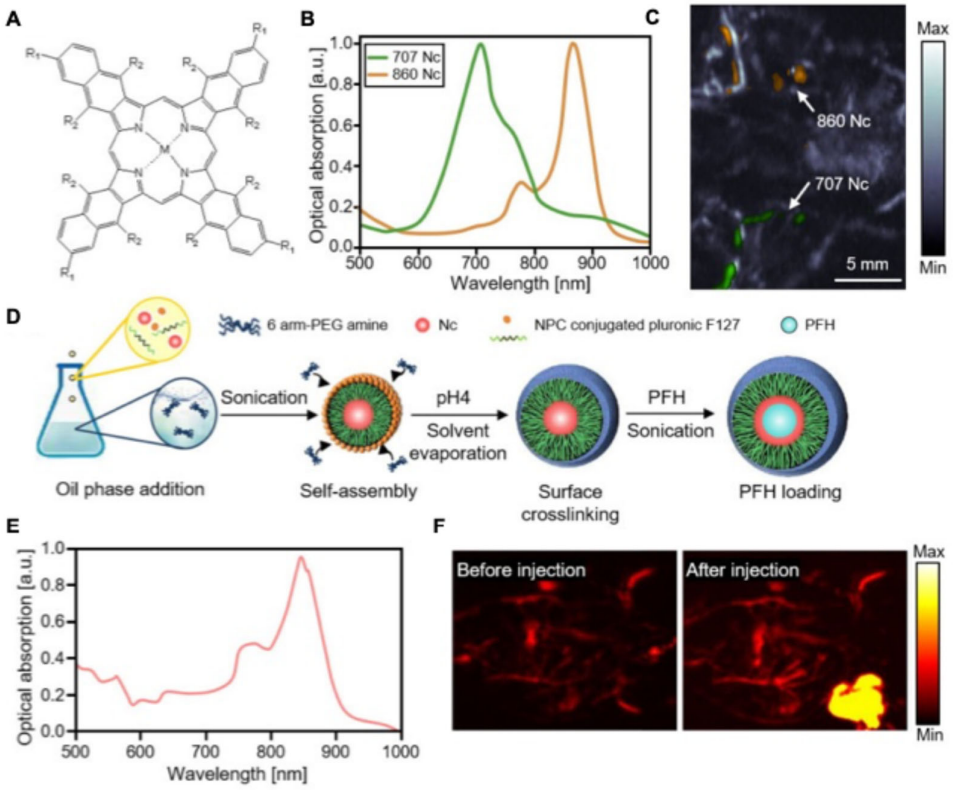

Figure 5. (A) Chemical structure for naphthalocyanine based PAI agent. Where for dye 707 Nc is formulated with M = Zn, R_1 = t-Bu, and R_2 = H, while 860 Nc is formulated with M = 2H, R_1 = H, and R_2 = O-$(CH_2)_3CH_3$. (B) optical absortionj spectra for various naphthalocyanine dyes. (C) Contrast-enhanced photoacoustic imaging of murine lymphatic vasculature following administration of nanoformulated naphthalocyanine dyes into the right and left forepaws. Photoacoustic signals corresponding to the nanoformulated dyes are displayed in green and orange, associated with absorption maxima at 707 and 860 nm, respectively. Reproduced with permission from[88]. Copyright 2015 Elsevier. (D) Schematic representation of the preparation of PFH-loaded naphthalocyanine nanostructures. (E) UV–vis–NIR absorption profile of naphthalocyanine dyes following encapsulation within PFH. (F) Photoacoustic images acquired before and after in vivo administration of the naphthalocyanine -PFH formulation, demonstrating enhanced contrast. Abbreviations: PA, photoacoustic; PFH, perfluorohexane; NPC, 4-nitrophenyl chloroformate. Reproduced with permission from [90]. Copyright 2019, American Chemical Society.

Fan et al. developed a near-infrared–absorbing PDI derivative by incorporating a tertiary amine donor and a diimide acceptor to enhance intramolecular charge transfer, followed by nanoparticle formulation using DSPE-mPEG-5000 to improve aqueous dispersibility[91]. The resulting PDI nanoparticles exhibited a narrow size distribution (~50 nm), strong NIR absorption around 700 nm, and excellent photostability and serum stability compared with indocyanine green. In vivo photoacoustic imaging demonstrated robust accumulation of these nanoparticles in orthotopic brain tumors through passive targeting, with PA spectra and three-dimensional ultrasound/PA imaging confirming selective localization and high-contrast tumor delineation.

Beyond tumor imaging, PDI nanoparticles have also been adapted for long-term cellular tracking. Stabilization of PDI nanoparticles using a star-shaped hyperbranched polymer matrix enabled persistent photoacoustic signals from labeled mesenchymal stromal cells for more than ten days after transplantation [92]. Importantly, control studies confirmed that the observed signals originated from viable labeled cells rather than secondary uptake by macrophages, supporting the suitability of PDI nanoparticles for reliable longitudinal cell tracking.

 doi:10.20944/preprints202602.0438.v1

Targeted vascular imaging has also been achieved through surface functionalization of PDI nanoparticles. Cui et al. modified PEGylated PDI nanoparticles with cyclic RGD peptides to selectively recognize GPIIb/IIIa receptors in early thrombus formation[93]. In a mouse thrombosis model, these probes generated significantly stronger PA signals in newly formed clots compared with older thrombi, enabling sensitive discrimination of thrombus stage. Photoacoustic imaging further allowed real-time monitoring of thrombolytic therapy, while conventional ultrasound and MRI showed limited sensitivity, highlighting the advantages of PDI-based PA probes for molecularly targeted vascular imaging.

5. SERS Based Imaging

Organic dyes possess well-defined vibrational signatures, making them effective Raman reporters for surface-enhanced Raman spectroscopy (SERS) in both bioanalytical detection and biomedical imaging [94,95]. When incorporated as Raman tags, these dyes enable highly sensitive and multiplexed identification of biomolecules, cells, and disease-associated markers [95]. Importantly, chemical modification of organic chromophores allows fine control over Raman intensity, resonance enhancement, and molecular targeting, supporting their use in selective diagnostic and imaging applications. In healthcare settings, dye-based Raman probes have been widely explored for cancer diagnosis, pathogen detection, and real-time monitoring of cellular behavior, offering high molecular specificity with minimal background interference[96]. Their integration with plasmonic nanostructures and targeted delivery systems continues to advance the clinical potential of Raman-based technologies in noninvasive diagnostics and precision medicine [97].

Among organic Raman reporters, BODIPY dyes have been extensively investigated for SERS applications due to their characteristic vibrational modes, including C–H stretching, C=C bonds, and B–N/C–N functionalities, which are strongly enhanced upon interaction with gold or silver nanoparticles[98,99]. Adarsh and co-workers developed a series of aza-BODIPY derivatives capable of adsorbing onto gold nanoparticle surfaces to generate robust SERS signals [99]. One derivative in particular exhibited high photostability and strong Raman response, enabling label-free discrimination of multiple human cancer cell lines through distinct Raman fingerprints without the need for specific surface markers. Three-dimensional Raman imaging and spectral analysis confirmed that the nanoprobe localized near the cell membrane, while no comparable signal was observed in normal fibroblast cells. Further conjugation of the probe with an epidermal growth factor receptor–targeting ligand improved cancer-cell specificity, enabling ultrasensitive and selective imaging. Beyond cancer detection, Raman-active dyes have also been applied to metabolic imaging. Klapper et al. demonstrated that Raman spectroscopy could be used to quantify lipid distribution and fat content in biological systems, where BODIPY-labeled lipid structures showed strong spatial correlation with Raman lipid signals [100]. Collectively, these studies highlight the versatility of organic dyes as Raman reporters for sensitive, targeted, and multifunctional healthcare applications.

SERS tags provide a powerful platform for probing local chemical environments and dynamic changes within living cells [101]. The strong electromagnetic enhancement generated by noble metal nanoparticles enables ultrasensitive and nondestructive detection of endogenous molecular species that are otherwise difficult to observe. By analyzing variations in SERS signals, subtle biochemical parameters—such as local pH and molecular composition—can be monitored at high spatial resolution. Pioneering studies by Kneipp and co-workers demonstrated this capability using dye-labeled gold and silver nanoparticles, including probes based on indocyanine green [102], rose Bengal [103], and crystal violet [104]. Upon cellular internalization, these SERS tags produced distinct vibrational fingerprints from both the reporter dyes and surrounding intracellular components. Importantly, spectral subtraction and analysis revealed Raman features associated with proteins, lipids, and nucleic acids in the immediate nanoparticle environment, highlighting the ability of SERS to extract localized chemical information from complex biological matrices at the single-cell level.

 doi:10.20944/preprints202602.0438.v1

SERS-based theranostic platforms have recently gained significant attention for their ability to integrate diagnostic imaging with therapeutic intervention. Bhatia and co-workers demonstrated this concept using near-infrared–responsive plasmonic gold nanorods (AuNRs) loaded with organic dyes for simultaneous tumor detection and photothermal therapy (Figure 6A) [105]. In their design, AuNRs were encoded with multiple Raman reporter dyes (DTTC-765, IR-792 and DTDC-655), enabling strong SERS signals that were several orders of magnitude higher than those obtained through conventional optical detection (Figure 6B). In vivo Raman imaging of mice bearing bilateral MDA-MB-435 tumors revealed pronounced signal enhancement from reporter-loaded nanorods, confirming effective tumor accumulation (Figure 6C). Upon irradiation with an 810 nm laser, tumors treated with either bare or SERS-encoded AuNRs rapidly reached temperatures sufficient for thermal ablation, while control tumors showed minimal heating (Figure 6D). These findings highlight the utility of SERS-coded plasmonic nanostructures as multifunctional agents capable of noninvasive tumor imaging and effective photothermal treatment within a single platform.

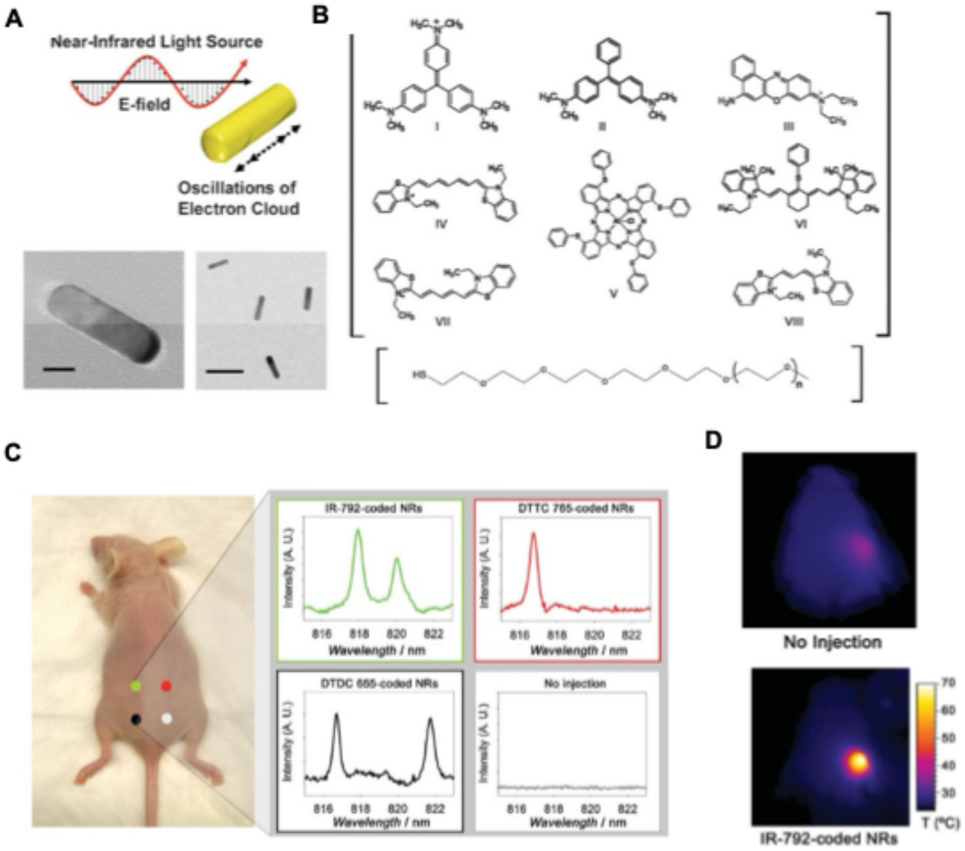

Figure 6. (A-B) Schematic representation and TEM micrographs illustrating the architecture of gold nanorods (AuNRs), including the incorporation of SERS reporter molecules and PEG chains to produce PEGylated, SERS-encoded NRs. Scale bars correspond to 10 nm (left) and 60 nm (right). (C) In vivo SERS imaging of three spectrally distinct nanorod formulations. The nanoparticles were injected subcutaneously at different locations in athymic (nu/nu) mice. Raman spectra were collected from each injection site and analyzed relative to background signals from untreated tissue areas. (D) Infrared thermal images depicting surface temperature changes in mice recorded 3 minutes after initiation of laser irradiation (810 nm diode laser, 2 W cm^{-2}). reproduced with permission from[105]. Copyright 2009, Wiley Publishers.

 doi:10.20944/preprints202602.0438.v1

6. Cardiovascular Imaging

Cardiovascular diseases are another life threat. Early detection and diagnosis are crucial for these diseases. Atherosclerosis a chronic inflammation condition, which creates vulnerable plaques which eventually forms fatty streaks, and their rupture cause thrombosis, severe health issues including blood loss, death [106]. Organic dyes have been used as a contrast agent to track such conditions sing various imaging techniques.

In one of the work Yu et al fabricated amphiphilic PDI NPs for aiming to diagnose early thrombus (Figure 7A) [93]. The assembled PDI molecules were conjugated with cyclic RGD peptide for selectively combining with Glycoprotein IIb/IIIa, an appropriate biomarker of early blood clot. Owing to the high PAI capability these nanoparticles were used for in vito and in vivo imaging to diagnostic early thrombus formation in live mice (Figure 7B-C). These NPs possess excellent stability, blood circulation and PA contrast intensity which is four times higher than control and blocking, and old thrombus groups. As shown in figure 7C, early thrombus formation was evaluated in an $FeCl_3$-induced murine jugular vein thrombosis model using ultrasound (US), MRI, and PAI. US revealed a vague wall-adherent protrusion in the thrombus-bearing vessel; however, poor intrinsic contrast made it difficult to clearly distinguish thrombus from surrounding tissue. T2-weighted MRI provided superior anatomical detail and vessel visualization, but small, non-occlusive thrombi did not generate discernible signal changes due to minimal effects on blood flow. In contrast, PAI enabled high-contrast, high-resolution visualization of the vasculature based on hemoglobin absorption. A marked loss of PA signal was observed at the thrombus site, consistent with local ischemia and reduced hemoglobin content. Compared with US and MRI, PAI allowed unambiguous detection of early thrombus, highlighting its strong potential for thrombosis imaging (Figure 7D). Nevertheless, the signal-off nature of thrombus in PAI underscores the need for targeted PA contrast agents to improve thrombus visualization and characterization.

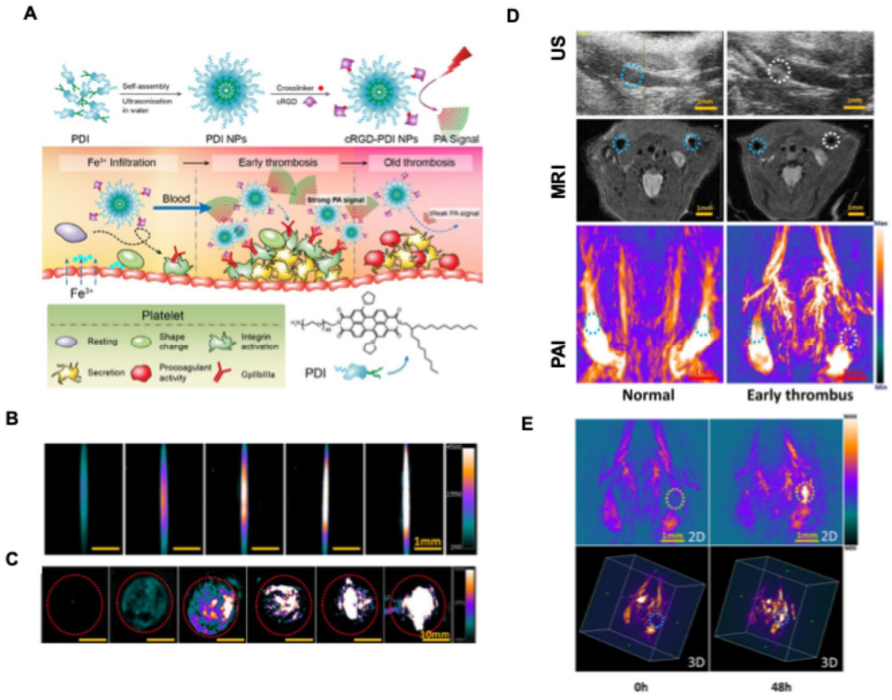

Figure 7. (A) Schematic representation of cRGD-PDI nanoparticle (NP) fabrication and the targeted photoacoustic imaging (PAI) strategy for selective visualization of early thrombus. (B) Photoacoustic responses of cRGD-PDI NPs in aqueous solution at concentrations of 0.125–2.000 mg mL^{-1}. (C) In vivo PAI following subcutaneous injection of cRGD-PDI NPs in mice (~0.5 mm depth) at concentrations of 0.0625–2.000 mg mL^{-1}, shown from left to right within red dashed regions. (D) Multimodal in vivo detection of early venous thrombosis

 doi:10.20944/preprints202602.0438.v1

using ultrasound (US), magnetic resonance imaging (MRI), and PAI. US images show normal jugular veins (blue circles) and thrombus-bearing veins (white circles). Corresponding transverse T2-weighted MRI scans (TR = 1206.9 ms, TE = 2.0 ms) and PAI confirm thrombus presence. Left panels represent healthy mice, while right panels show $FeCl_3$-induced thrombus models, with thrombosis generated only in the right jugular vein. (E) Longitudinal PAI of early thrombus regions (yellow dashed lines in 2D images and blue dashed lines in 3D reconstructions) immediately after injection and 48 h post-administration of cRGD-PDI NPs. Reproduced with permission from [93]. Copyright 2017, American Chemical Society.

Li et al. developed a NIR-II dye, LZ-1105, that exhibits both absorption and emission beyond 1000 nm [107]. Owing to its long blood circulation half-life (~3.2 h), this probe was successfully applied for imaging ischemia–reperfusion in hindlimb models, monitoring thrombolysis in the carotid artery, and visualizing the opening and subsequent recovery of the blood–brain barrier. In another study Sun et.al used J-aggregates from cyanine dye FD-1080 for the NIR-II in Vivo Dynamic Vascular Imaging beyond 1500 nm [108]. These aggregates enabled continuous, real-time imaging of carotid artery diameter in the >1500 nm NIR window following intravenous administration of the J-aggregates together with a hypotensive agent in spontaneously hypertensive rats. Quantitative analysis based on the full width at half maximum of cross-sectional intensity profiles revealed a marked increase in carotid artery width from approximately 370 to 680 μm within 240 s. In parallel, arterial blood pressure was independently monitored using a clinically approved blood pressure device, which showed a reduction in systolic pressure from 180 to 134 mmHg within 280 s. These results demonstrate a clear correlation between vessel dilation and decreasing blood pressure following Isoket administration. This study represents the first demonstration of real-time evaluation of hypotensive efficacy through direct monitoring of vascular diameter changes using NIR-II imaging.

Shimizu and colleagues developed ICG–derived fluorescent probe, termed Peptide-ICG2, for NIR imaging of macrophage-rich atherosclerotic lesions [109]. This probe functions as an activatable “turn-on” system in which fluorescence is initially suppressed by a peptide linker. Upon enzymatic cleavage by lysosomal cathepsin B, the quenching effect is removed, resulting in fluorescence activation. To enhance plaque targeting, Peptide-ICG2 was further incorporated into phosphatidylserine-containing liposomes (P-ICG2-PS-Lip), leveraging the affinity of phosphatidylserine receptors expressed on macrophages that preferentially localize within embolism-prone plaques. This liposomal formulation promoted selective uptake by macrophages and enabled intracellular fluorescence activation, allowing effective NIR visualization of vulnerable atherosclerotic regions. In a separate study, Kim and Chang et al. introduced a low-molecular-weight fluorescent probe, CDg16, designed to selectively recognize activated macrophages[110]. In vivo studies demonstrated that CDg16 effectively highlighted inflammatory sites in atherosclerotic tissue through direct targeting of macrophage populations. Detailed transporter screening revealed that probe uptake occurs via the SLC18B1 transporter, providing mechanistic insight into its selective staining behavior. Collectively, these studies present promising molecular imaging strategies for detecting macrophage-driven inflammation and advancing diagnostic approaches for inflammation-associated diseases.

7. Light Based Therapy

Organic dyes absorb light at specific wavelengths and dissipate the absorbed energy through heat generation or via secondary photochemical processes that produce reactive oxygen species (ROS)[111]. These mechanisms form the basis of photothermal therapy (PTT) and photodynamic therapy (PDT), where tumor ablation is achieved through localized heating or ROS-mediated cytotoxicity [14,15,112].

Upon near-infrared (NIR) excitation, organic dyes undergo absorption followed by electronic transitions that can be described using the Jablonski diagram (Figure 8)[113]. Light absorption promotes an electron from the ground singlet state (S_0) to an excited singlet state (Sn), which rapidly

 doi:10.20944/preprints202602.0438.v1

relaxes to the lowest excited singlet state (S_1). From S_1, the molecule can follow three competing pathways: radiative decay producing fluorescence, non-radiative relaxation generating heat, or intersystem crossing to the triplet state (T_1), which can subsequently yield ROS through energy transfer to molecular oxygen. These pathways underpin fluorescence imaging, PTT, and PDT, respectively. The balance among fluorescence emission, thermal dissipation, and ROS generation is governed by molecular structure and electronic properties. Rigid molecules with large energy gaps tend to favor radiative decay, whereas flexible structures or donor–acceptor systems with strong intramolecular charge transfer enhance non-radiative decay and intersystem crossing. While donor–acceptor architectures can improve ROS generation for PDT, they may suppress fluorescence or reduce photothermal efficiency. Therefore, rational molecular design is essential to optimize NIR dyes for combined imaging and synergistic PTT–PDT applications, particularly in overcoming limitations such as tumor hypoxia, light penetration depth, and photosensitizer localization.

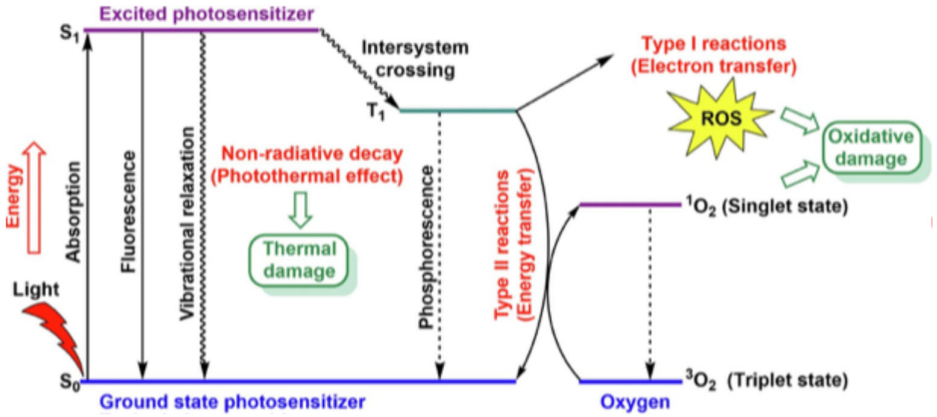

Figure 8. Jablonski diagram illustrating the photophysical pathways underlying photodynamic therapy (PDT) and photothermal therapy (PTT). Upon light absorption, the photosensitizer (PS) is excited from the ground state (S_0) to the singlet excited state (S_1). The PS can relax back to S_0 via fluorescence emission or nonradiative decay, producing heat for PTT. Intersystem crossing populates the triplet state (T_1), which reacts with molecular oxygen ($^3O_2$) to generate singlet oxygen ($^1O_2$) through a Type II process, or produces reactive oxygen species (ROS) via Type I electron-transfer reactions. These ROS induce oxidative cellular damage. Abbreviations: PDT, photodynamic therapy; PTT, photothermal therapy; PS, photosensitizer; ROS, reactive oxygen species; S_0, S_1, ground and singlet excited states; T_1, triplet excited state; $^3O_2$, molecular oxygen; $^1O_2$, singlet oxygen. Reproduced with permission from [113]. Copyright 2024, Springer Nature.

7.1. Dyes for Photothermal Therapy Applications

NIR dyes can be used directly as photothermal agent. FDA approved dye ICG is used first directly as PT agent for tumor ablation. Studies showed that ICG+laser irradiation showed a large decrease in tumor volume than saline+laser. But the half-life of ICG is very small approximately 3 minutes, so the irradiation study might be performed fast after the tail vein injection [114]. Controlling the temperature and long-term accumulation of PT agents are still challenging. Recently these organic dyes have used along with other nanoformulations for improved solubility, targeting capability and reduce the dose of these dyes for PTT applications. IR-780 iodide dye which is a class of cyanine dye known for its NIR absorption and emission, lack solubility in most of the biological media. It was shown that encapsulation of this dye into PEG–PCL (Poly(ethylene glycol)-Polycaprolactone) micelles, improved their in vivo imaging assisted PTT[115]. One of the challenges for using organic dyes for PTT applications is their inherent photobleaching and degradation property under lase irradiation. To control this a variety of cyanine dyes were developed by controlling their photoinduced electron transfer property with various substituents. These dyes

 doi:10.20944/preprints202602.0438.v1

showed enhanced photothermal conversion efficiencies up to 34.5% as compared with the unsubstituted derivatives.

Recently image guided PTT become an advance cancer treatment modality in which the contrast agent can guide the clinicians for visualization of tumor and precise laser-based therapy can be performed. One of the recent studies by Hassan et al. showed use of NIR-II dye (IR1116) as an effective photothermal agent with a photothermal conversion efficacy of 79% [116]. The dye structure contains donor-acceptor units which control the photooxidation and stability. To improve water solubility DSPEPEG is used and a nanoformulation was prepared which they called as nano heater. In vitro and in vivo studies on 4T1 breast cancer showed tumor cell apoptosis under 1064 nm laser irradiation for1 minute. The dye showed promising results for tumor ablation in both NIR-I and NIR-II conditions.

BODIPY-based chromophores have emerged as highly efficient photothermal agents, particularly when engineered to operate in the near-infrared (NIR) region, where light penetration through biological tissues is maximized while minimizing off-target damage [14]. One of the key advantages of these dyes lies in their modular molecular architecture, which enables fine control over absorption wavelengths to meet the requirements of photothermal therapy (PTT). In PTT, localized heat generation induces cancer cell death through hyperthermia and the activation of heat-shock protein–mediated pathways[117]. Due to their strong NIR absorbance, BODIPY derivatives are well suited for treating deep-seated tumors[118]. Notably, π-conjugation extension in BODIPY scaffolds has led to photothermal conversion efficiencies exceeding 90%, demonstrating exceptional light-to-heat conversion performance (Figure 9A) [119]. Upon exposure to an 808 nm laser (0.75 W cm^{-2}), aqueous suspensions of meso-CF_3-substituted BODIPY nanoparticles (20 μM dye concentration) exhibited rapid temperature elevation, reaching peak values of 66.8 °C (ΔT = 43 °C, TCF3PEn), 64.9 °C (ΔT = 41 °C, TCF3MEn), and 64.3 °C (ΔT = 41 °C, DCF3MEn) within 5 minutes (Figure 9B). Both in vitro and in vivo evaluations using an MCF-7 xenograft tumor model confirmed substantial therapeutic efficacy, with approximately 50% tumor volume reduction following treatment. Among the derivatives tested, the meso-CF_3-functionalized BODIPY (TCF3M) demonstrated superior apoptotic induction and tumor suppression under low-power NIR irradiation (808 nm, 0.3 W cm^{-2}), outperforming its structural analogs (Figure 9C).

Complementary studies by Li and co-workers further validated the therapeutic potential of aza-BODIPY derivatives, reporting photothermal conversion efficiencies in the range of 48–50% along with pronounced cytotoxic effects against human colon cancer cells [101]. In a related investigation, Liu et al. developed an aza-BODIPY compound exhibiting strong absorption at 781 nm, high photostability, and robust photothermal performance [120]. Photothermal measurements revealed a concentration-dependent heating effect, with temperatures rising to 74.5 °C at a dye concentration of 35 μg mL^{-1} after 5 minutes of laser exposure. Correspondingly, laser-activated cytotoxicity assays showed a clear dose-dependent reduction in CT26 cell viability. In vivo fluorescence imaging combined with PTT demonstrated rapid temperature increases of up to 44.9 °C within 1 minute, resulting in tumor growth inhibition of approximately 96% following intratumoral administration and 89% after systemic delivery. Importantly, treated animals exhibited normal weight gain post-therapy, indicating minimal systemic toxicity. In another example, Pewklang et al. reported an aza-BODIPY-pyrazole derivative displaying intense NIR absorption around 900 nm and a photothermal conversion efficiency approaching 33% [121]. Confocal imaging confirmed efficient cellular uptake within 6 hours, while subsequent PTT experiments achieved nearly 70% cancer cell eradication. Beyond oncological applications, this dye also demonstrated potent antibacterial activity, achieving complete elimination of Escherichia coli 780 and Staphylococcus aureus 1466 upon laser irradiation.

 doi:10.20944/preprints202602.0438.v1

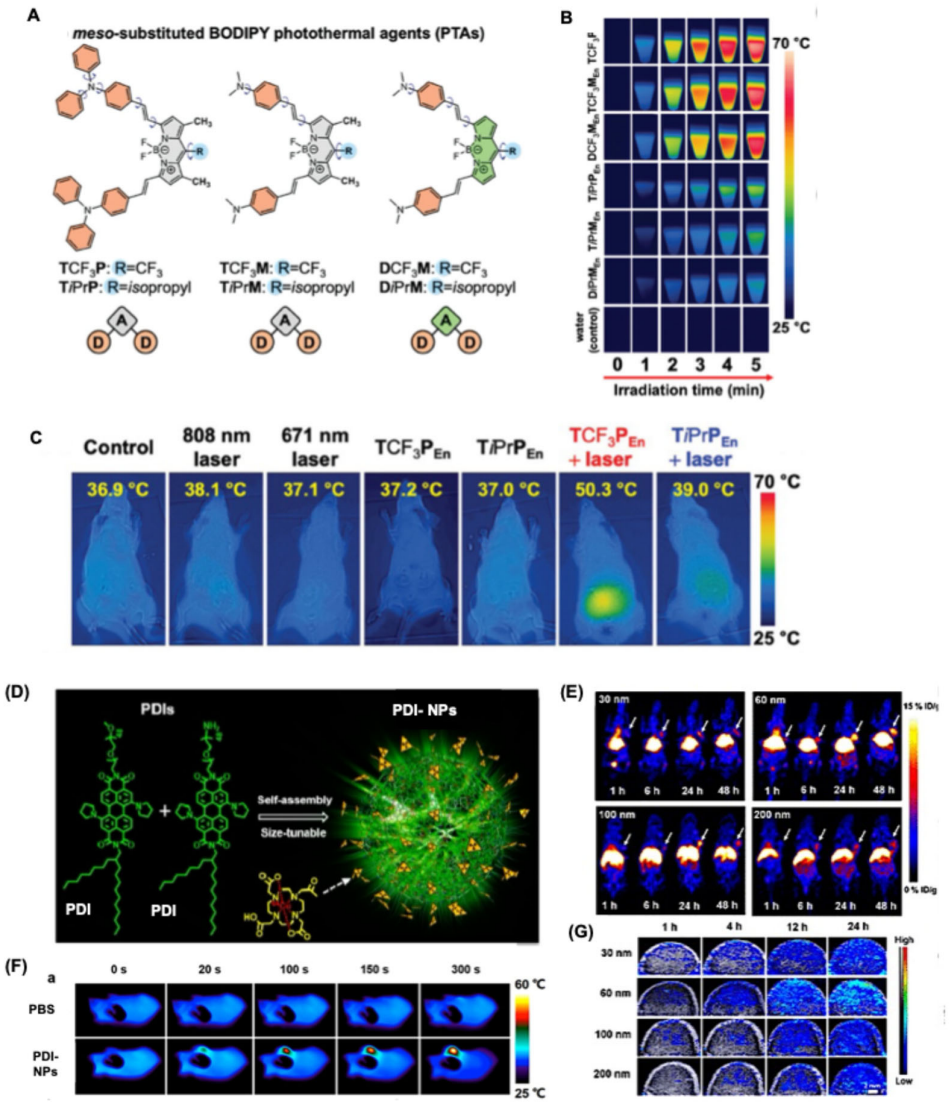

Figure 9. (A) Molecular structures of the synthesized BODIPY dye series. (B) Infrared thermographic images of BODIPY dyes exposed to 808 nm laser irradiation (0.75 W cm^{-2}), showing a pronounced temperature increase for TCF3MEn and TCF3PEn. (C) In vivo thermal infrared imaging of tumor-bearing mice after intratumoral administration of TCF3PEn or TiPrPEn (15 μM, 2 h incubation), or control treatment, followed by laser irradiation at 0.3 W cm^{-2} for 5 min, highlighting temperature changes at the tumor region. Reproduced with permission from [119]. Copyright 2024, Wiley. (D) Schematic illustration of the self-assembly strategy used to fabricate PDI-58 nanoparticles. (E) Decay-corrected coronal PET images acquired at 1, 6, 24, and 48 h after intravenous injection of PDI- nanoparticles with different sizes; U87MG tumors are marked by white arrows. (F) Infrared thermal images of U87MG tumor–bearing mice under 675 nm laser irradiation (1 W cm^{-2}) at 24 h following administration of PBS or PDI- nanoparticles. (G) Overlayed coronal photoacoustic (PA) and ultrasound (US) images of U87MG tumors collected at 1, 4, 12, and 24 h post-injection of size-controlled PDI-nanoparticles. Reproduced with permission from [122]. Copyright 2017, American Chemical Society.

Self-assemble PDI derivatives also used for PTT applications [15]. Various J and H-aggregates from PDI derivatives showed interesting photophysical properties, and high photothermal conversion efficiencies. Recently Yan et al prepared self-assembled PDI derivatives with varying sizes 30, 60, 100, and 200 nm by adjusting the initial PDI concentration (Figure 9D) [122]. Among these the NPs with size 60 nm showed enhanced tumor targeting, and photothermal conversion efficiency

 doi:10.20944/preprints202602.0438.v1

(Figure 9E, F). These NPs were used as PA probes and photothermal agents, with size-dependent aggregation being observed in tumors through PA and PET imaging using [64Cu]-labeling. After 10 days the results showed complete elimination of tumor via PTT (Figure 9G). Yang et al. reported a photoresponsive theranostic nanoplatform (HMPDI@TP-SN38) for imaging-guided photothermal–chemotherapy using an in situ skeleton growth strategy[123]. The nanoparticles were prepared by co-hydrolyzing PEG2000–PDI–silane with silica precursors, followed by selective ammonia etching to remove the mesoporous silica core and generate a hollow PDI shell. Subsequent grafting of thermosensitive polymers enhanced fluorescence and photoacoustic signals while enabling efficient drug tracking. Under NIR irradiation, PDI-mediated photothermal heating induced polymer contraction and triggered controlled SN38 release, reducing premature leakage and improving drug loading efficiency. This integrated nanotheranostic system enables real-time visualization of drug distribution and precise, on-demand therapy. Other dyes such as Rhodamine, Porphyrin, Diketopyrrolopyrrole etc. were also used for PTT and image guided therapy[112].

7.2. Organic Dyes for Photodynamic Therapy (PDT)

Photodynamic therapy (PDT) is a light-activated cancer treatment that requires a photosensitizer (PS), oxygen, and an external light source [124]. Upon excitation, the PS relaxes through fluorescence emission, heat dissipation, or intersystem crossing to a triplet excited state, as described by the Jablonski diagram (Figure 8). The triplet state reacts with oxygen to generate singlet oxygen via Type II processes or reactive oxygen species (ROS) through Type I pathways. These cytotoxic species induce tumor cell death through apoptosis, necrosis, and autophagy while also stimulating antitumor immune responses an effective PS should selectively accumulate in tumors, exhibit minimal dark toxicity, maintain chemical stability, efficiently generate singlet oxygen, and be activatable within the 680–800 nm window to enable deeper tissue penetration.

Barbero et al. reported a series of pentamethine NIR cyanine dyes engineered for photodynamic therapy [125]. Structural modifications, including bromination of the benzoindolenine unit and alkyl substitution at the C2/C4 positions, enhanced singlet oxygen generation and light-induced cytotoxicity. All dyes displayed sharp NIR absorption within the therapeutic window and showed strong phototoxic effects at low concentrations in HT-1080 cells, while bromine substitution had minimal influence on overall PDT efficiency, supporting their in vivo potential. Peng et al. later developed a water-soluble aminocyanine dye incorporating a TEMPO radical to promote efficient intersystem crossing[126]. This design resulted in a prolonged triplet-state lifetime (≈9.16 μs), a large Stokes shift (~100 nm), and NIR absorption/emission suitable for biological applications. Time-resolved spectroscopy confirmed oxygen-sensitive long-lived triplet states, enabling efficient singlet oxygen generation. In vitro studies demonstrated high phototoxicity with negligible dark toxicity, with AO/EB staining indicating apoptosis as the primary cell-death mechanism, highlighting dye 5 as a promising PDT candidate for future biomedical applications.

Conventional BODIPY dyes show strong singlet oxygen generation with heavy atom substitution such as iodine, bromine to their backbone. This will enhance the intersystem crossing efficiency of BODIPY dyes, allow various secondary process such as singlet oxygen and ROS generation. In 2016, Kim and co-workers reported the development of a halogenated BODIPY photosensitizer designed to enhance photodynamic performance [127]. In acetonitrile, this dye displayed well-defined absorption and emission maxima at 528 nm and 546 nm, respectively, accompanied by a low fluorescence quantum yield ($\Phi F \approx 0.02$), indicative of efficient nonradiative deactivation pathways. Direct near-infrared luminescence measurements revealed intense singlet oxygen emission at 1270 nm, with an exceptionally high singlet oxygen quantum yield ($\Phi\Delta \approx 0.93$). This remarkable efficiency was attributed to the heavy-atom effect introduced by iodine substitution at the 2- and 6-positions, which significantly promoted intersystem crossing to the triplet excited state. Biological evaluation in LLC cells showed minimal dark toxicity, with cell viability remaining above 70% at concentrations up to 15 μmol L^{-1}, while light irradiation (3.5 mW cm^{-2}) induced

 doi:10.20944/preprints202602.0438.v1

substantial cytotoxicity, reducing viability to approximately 50% at 10 μmol L^{-1}. These results highlight this dye as a highly effective and biocompatible light-activated photosensitizer.

PDT-induced hypoxia remains a major limitation of photodynamic therapy, as it can activate angiogenic pathways that promote tumor recurrence and reduce therapeutic efficacy. To address this challenge, Jung et al. developed an acetazolamide-conjugated BODIPY photosensitizer (AZ-BPS) that integrates anti-angiogenic activity with PDT and BODIPY sensitizer (BPS) as a control molecule (Figure 10 A) [128]. AZ-BPS showed strong absorption at 661 nm and emission at 689 nm, with a fluorescence quantum yield of 0.06 and a singlet oxygen quantum yield of 0.6, comparable to clinically used photosensitizers. The probe was photostable in PBS containing 10% DMSO. Notably, the dye selectively targeted carbonic anhydrase IX (CAIX), a hypoxia-associated enzyme overexpressed in tumors. CAIX-high MDA-MB-231 cells exhibited significantly higher uptake and fluorescence than CAIX-low MCF-7 cells (Figure 10B). Upon 660 nm laser irradiation, AZ-BPS induced extensive phototoxicity in MDA-MB-231 cells, with ~92.5% undergoing late apoptosis or necrosis. In tumor-bearing mice, PDT treatment with AZ-BPS resulted in markedly reduced CD31 expression, indicating effective suppression of hypoxia-driven angiogenesis. Overall, this dual-functional design highlights the potential of combining PDT with anti-angiogenic targeting to improve cancer therapeutic outcomes (Figure 10C, D).

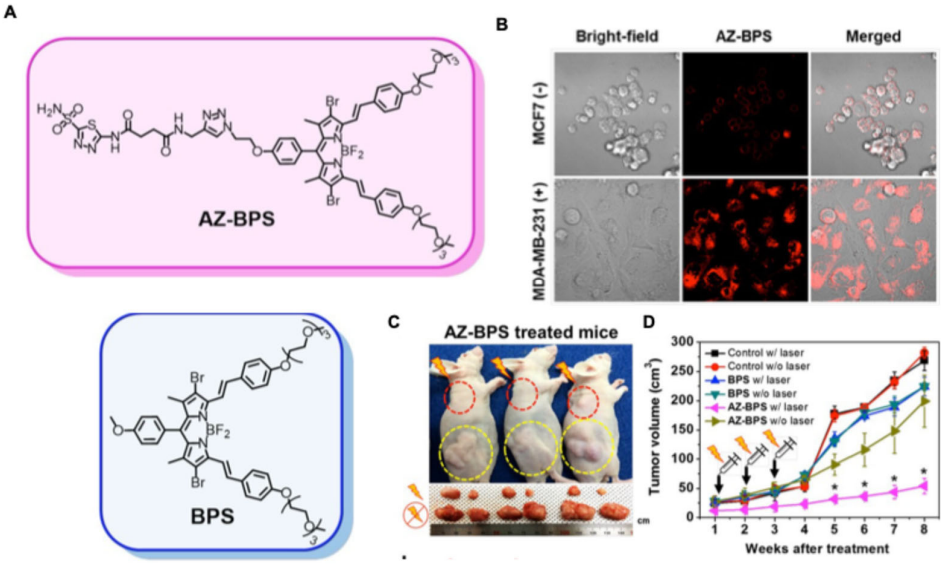

Figure 10. (A) Molecular structures of the photosensitizer AZ-BPS and the reference compound BPS used for photodynamic therapy studies. (B) Confocal fluorescence microscopy images of MDA-MB-231 and MCF-7 breast cancer cells after 4 h incubation with AZ-BPS (5 μM). (C) Top: Representative photographs of nude mice collected 8 weeks after intravenous administration of AZ-BPS, followed by localized irradiation of the upper tumor (red dashed circle) using a 660 nm laser (2.0 W cm^{-2}, 30 min; total dose 3600 J cm^{-2}). The contralateral lower tumor (yellow dashed circle) served as the non-irradiated control. Bottom: Excised tumors harvested from each treatment group. (D) Tumor growth curves of mice treated with BPS or AZ-BPS, with and without photodynamic therapy. Reproduced with permission from [128]. Copyright 2017, American Chemical Society.

In photodynamic therapy (PDT), hybrid nanoplatforms combining gold nanoparticles (AuNPs) with BODIPY dyes have demonstrated notable improvements in both therapeutic efficacy and bioimaging performance. Kumar and co-workers reported a series of rationally designed AuNP–BODIPY systems, highlighting how modulation of structure–activity relationships enable fine control over the photophysical behavior and fluorescence characteristics of these nanomaterials for diverse biomedical applications [129]. In their approach, tryptophan-reduced AuNPs served as a biocompatible scaffold onto which unmodified BODIPY dyes were immobilized through supramolecular interactions (Figure 11A). The resulting assemblies exhibited markedly improved

 doi:10.20944/preprints202602.0438.v1

photostability, suppressed fluorescence emission, and efficient singlet oxygen generation, with a quantum yield (ΦΔ) of 0.46. Notably, these nanostructures produced strong PDT-induced cytotoxicity against C6 glioma cells (~85% cell death) while maintaining negligible toxicity toward healthy cells (Figure 11B, C) . Building on this concept, the same group further explored the interplay between BODIPY molecular structure and energy-transfer processes by developing a series of Förster resonance energy transfer (FRET)-based nanocomposites [130]. In this system, NC1 consisted of pentamethyl BODIPY (1) coupled to AuNPs, NC2 employed an iodinated pentamethyl BODIPY derivative (2), and NC3 incorporated both BODIPY dyes simultaneously within a single AuNP framework. Upon photoexcitation, NC3 displayed enhanced surface-associated luminescence arising from an alternative radiative decay pathway, enabling concurrent fluorescence imaging and PDT (Figure 11D-E). This dual-dye nanocomposite achieved a high singlet oxygen quantum yield (ΦΔ = 0.68), comparable to that of methylene blue, while offering superior photostability relative to the free dye [120]. Beyond therapy, AuNP–BODIPY assemblies have also been engineered for intracellular sensing applications. Because tumor cells typically exhibit elevated levels of biothiols, an indicator displacement strategy was developed in which BODIPY fluorescence was initially quenched upon adsorption to the AuNP surface. Interaction with cellular biothiols displaced the dye from the metallic interface, restoring fluorescence and generating a distinct “turn-on” signal (Figure 11F). This responsive platform enabled effective cancer cell imaging as well as quantitative assessment of intracellular biothiol concentrations, demonstrating the multifunctional potential of AuNP–BODIPY nanoconstructs in oncological diagnostics and therapy [131,132].

Phthalocyanines (Pcs) are well-established second-generation photosensitizers for photodynamic therapy (PDT) owing to their strong near-infrared (NIR) absorption, favorable photostability, and efficient singlet oxygen generation[111]. Zinc and silicon phthalocyanines (ZnPcs and SiPcs) are the most widely explored Pc platforms, with several derivatives demonstrating dual functionality in imaging and PDT[133]. ZnPcs exhibit intense NIR fluorescence suitable for optical and nuclear imaging, while maintaining high photodynamic efficiency[134]. Structural modification of Pc cores has enabled enhanced cellular uptake, subcellular targeting, and tumor selectivity, resulting in promising in vitro and preliminary in vivo PDT outcomes[135]. Targeted Pc designs have further expanded PDT efficacy by exploiting tumor-specific biological features. Mitochondria-directed SiPc conjugates achieved efficient intracellular localization and strong one- and two-photon phototoxicity, highlighting the advantage of organelle-specific PDT[136]. Similarly, biotin-functionalized SiPcs selectively accumulated in biotin receptor–overexpressing cancer cells, producing potent light-induced cytotoxicity with minimal dark toxicity[137]. Peptide-mediated targeting using cyclic RGD motifs enabled selective recognition of integrin $\alpha v\beta 3$-overexpressing tumors, resulting in enhanced tumor uptake and significant tumor growth inhibition in vivo[138]. Collectively, these studies demonstrate that rational functionalization of phthalocyanines enables multifunctional, tumor-selective photosensitizers with strong potential for image-guided PDT.

Beyond cyanines, BODIPYs, and phthalocyanines, a range of emerging chromophores have been reported as alternative photosensitizers. Rhodamine-based systems, valued for their chemical robustness and optical brightness, have been extensively modified to create next-generation PDT agents[139,140]. Selenium-containing rhodamine derivatives exploit the internal heavy-atom effect to enhance intersystem crossing [141]. Piao et al. developed a hypoxia-activated seleno-rosamine photosensitizer incorporating an azo linker that suppressed singlet oxygen generation under normoxic conditions (ΦΔ ≈ 0.03) but was selectively cleaved under hypoxia to release the active dye (ΦΔ ≈ 0.56) [141]. Upon light irradiation, treated A549 cells exhibited marked cytotoxicity under hypoxia, with cell viability reduced to ~40%, and effective PDT was observed even at ~8% oxygen.

 doi:10.20944/preprints202602.0438.v1

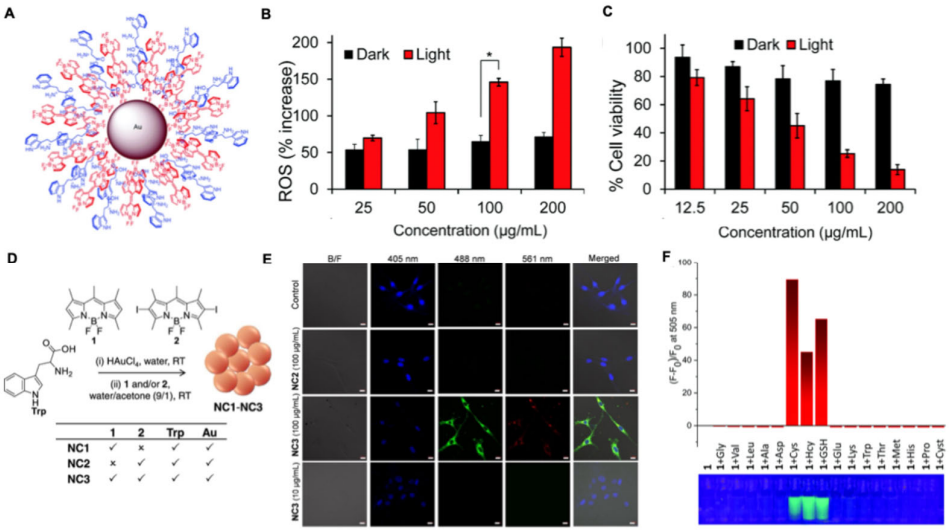

Figure 11. (A) (A) Conceptual schematic illustrating the assembly of a Pyrrole-BODIPY/tryptophan–gold nanocomposite. (B) Quantitative analysis of intracellular reactive oxygen species (ROS) generation in C6 glioma cells following treatment with Pyrrole-BODIPY–Au nanoparticles. (C) Cell viability of C6 cells exposed to Pyrrole-BODIPY–Au nanoparticles under dark conditions and upon white LED irradiation (36 W). Statistical significance was determined using a two-tailed test (*p = 0.0001). reproduced with permission from [129]. Copyright 2019, RSC publishers. (D) Design scheme of hybrid nanocomposites constructed from two distinct BODIPY chromophores and gold nanoparticles. The accompanying table summarizes the formulations of nanocomposites NC1, NC2, and NC3. Energy transfer processes, including Förster resonance energy transfer (FRET) and electron transfer from aggregated BODIPY units (1 and 2) to gold, enable simultaneous fluorescence modulation and singlet oxygen production. (E) Confocal laser scanning microscopy images of C6 glioma cells treated with nanocomposites NC2 and NC3. Bright-field (B/F) images and fluorescence channels were acquired using 405, 488, and 561 nm excitation lasers. Scale bar: 10 μm. Reproduced with permission from [130]. Copyright 2022, American Chemical Society. (F) Mechanistic illustration of fluorescence activation (“turn-on”) triggered by biothiol interactions with BODIPY–Au nanocomposites. The nanoparticles are initially non-emissive due to gold-induced quenching; displacement of BODIPY dyes from the gold surface upon biothiol binding restores fluorescence emission. Reproduced with permission from [132]. Copyright 2020, RSC publishers.

Tumor-enzyme activation has also been used to improve selectivity. Chiba and co-workers designed a γ-glutamyltranspeptidase (GGT)–responsive selenorhodamine pro-photosensitizer that remained photoinactive until enzymatic cleavage in GGT-overexpressing tumors[142]. This system produced strong fluorescence recovery, efficient singlet oxygen generation, and selective phototoxicity in high-GGT cancer models, while causing minimal damage to normal tissues in chick chorioallantoic membrane assays. In another approach, a carbazole-based iodinated photosensitizer exhibited enhanced DNA-associated fluorescence in cancer cells, leading to light-dependent viability reduction to ~60% at 20 μM and significant tumor growth inhibition in vivo[143].

To overcome aggregation-caused quenching commonly observed in planar photosensitizers, aggregation-induced emission (AIE) materials have gained prominence. Mitochondria-targeted AIE photosensitizers combining tetraphenylethylene and triphenylphosphonium groups showed strong intracellular accumulation, pronounced fluorescence enhancement upon aggregation, and irradiation-dependent cytotoxicity[144]. Notably, this derivative displayed both photo- and chemo-cytotoxicity, enabling combined imaging, PDT, and chemotherapy without external drug conjugation. Multifunctional AIE systems have further enabled real-time therapy monitoring. Yuan et al. reported an AIE-active photosensitizer linked to a rhodol dye via a singlet oxygen-cleavable aminoacrylate linker and functionalized with cRGD for enhanced tumor uptake[145]. This probe

 doi:10.20944/preprints202602.0438.v1

exhibited a high singlet oxygen quantum yield (ΦΔ ≈ 0.68), substantially exceeding that of Photofrin, and allowed real-time fluorescence tracking of singlet oxygen generation during PDT.

Recent designs have expanded AIE scaffolds beyond tetraphenylethylene. A water-soluble NIR AIEgen displayed strong aggregation-dependent emission at ~708 nm, an exceptionally high singlet oxygen yield (~80%), and potent PDT efficacy, reducing HeLa cell viability to ~15% at sub-micromolar concentrations[146]. Following intratumoral injection, this probe enabled clear tumor imaging and effective cancer ablation in mouse models, while remaining non-fluorescent in aqueous environments to minimize background interference. Similarly, mitochondria-targeted AIE photosensitizers generated high levels of reactive oxygen species (ROS) and eliminated ~80% of A549 cells upon light irradiation, with successful mitochondrial imaging demonstrated in both cells and zebrafish embryos[147]. Stimuli-responsive theranostic systems have further improved PDT precision. Hu and co-workers developed a nitric oxide (NO)–activatable photosensitizer with a large two-photon absorption cross-section (~3300 GM)[148]. Upon exposure to elevate NO levels, fluorescence intensity increased ~18-fold and singlet oxygen generation reached ~82%. Two-photon irradiation reduced activated macrophage viability to ~19%, highlighting its potential for inflammation-associated cancer therapy.

Far-red and NIR AIE luminogens with strong donor–acceptor architectures have also been reported, displaying high solid-state quantum yields (up to ~30%), large Stokes shifts, and deep tissue imaging capability (>150 μm). Among these, a mitochondria-targeted derivative reduced cancer cell viability to ~10% at micromolar concentrations, outperforming commercial chlorin-based photosensitizers [149]. Additional non-AIE strategies include quinacridone derivatives capable of rapid ROS generation and photo-induced DNA cleavage, reducing cell viability to ~30% after seconds of irradiation and achieving effective tumor growth suppression in vivo[150]. To address hypoxia-induced PDT resistance, Nile blue–based heavy-atom-modified photosensitizers were developed to generate superoxide radicals via oxygen-independent Type I photoreactions[151]. These systems achieved up to ~94% cancer cell killing under hypoxic conditions and demonstrated strong tumor selectivity and renal clearance in vivo.

8. Dyes for Intraoperative Surgery Guidance and Therapy

Imaging-guided cancer therapy offers a unified framework that combines diagnosis and treatment, enabling real-time tumor monitoring, in situ acquisition of disease-specific information, and precise delivery of therapeutic agents. Organic dye-based theranostic platforms have been extensively developed to support near-infrared fluorescence and photoacoustic imaging, as well as multimodal image-guided surgery and light-activated therapeutic strategies, including PDT, PTT, and chemotherapy[152]. Leveraging external light activation, these approaches enable minimally invasive, high-efficiency treatments with reduced collateral damage. Intraoperative optical molecular imaging offers sensitive and specific visualization of tumor margins, facilitating accurate surgical resection, while advances in NIR-I/NIR-II multispectral imaging and combinatorial approaches incorporating PDT, PTT, or immune checkpoint blockade have demonstrated improved survival and strong translational potential, despite remaining limitations in penetration depth and targeting specificity[153,154].

An activatable cyanine probe emitting in the NIR-I window was reported to achieve an exceptionally high tumor-to-normal tissue contrast, enabling improved detection of metastatic lesions and facilitating image-guided surgical procedures (Figure 12A)[155]. The specific dye traget the CD13/aminopeptidase N (APN) a specific cancer marker. The dye used to distinguish normal and tumor cells accurately in a spraying manner to achieve fluorescent superior tumor-to-normal (T/N) tissue ratios (subcutaneous transplantation tumor, 13.86; hepatic metastasis, 4.42 and 6.25; splenic metastasis, 4.99) (Figure 12B). In comparison with conventional NIR-I fluorescence-guided surgery currently used in clinical practice, combined NIR-I and NIR-II multispectral imaging provided superior sensitivity, enhanced signal-to-noise ratios, and improved diagnostic specificity[156]. In a separate study, chlorin e6 (Ce6) was co-administered with either single or multiple immune checkpoint–blocking monoclonal antibodies to enable fluorescence-guided photodynamic therapy

 doi:10.20944/preprints202602.0438.v1

alongside immunotherapy during surgery(Figure 12C)[157]. This integrated intraoperative strategy, based on red-light fluorescence imaging, significantly extended survival in tumor-bearing mice and elicited durable immune memory responses, highlighting its translational promise for glioma and colorectal cancer treatment (Figure 12D, E). Collectively, these findings underscore the strong clinical potential of intraoperative fluorescence-guided PDT, PTT, and checkpoint inhibition approaches. However, optical molecular imaging remains constrained by limited tissue penetration and insufficient targeting precision, emphasizing the need for next-generation imaging probes that offer greater accuracy and specificity for real-time surgical cancer imaging.

Chemotherapy remains a cornerstone of cancer treatment; however, its clinical effectiveness is often limited by poor bioavailability, nonspecific distribution, and systemic toxicity. Incorporation of organic dyes into chemotherapeutic systems enables real-time visualization of drug biodistribution and therapeutic response, thereby enhancing treatment precision[152]. Advances in nanotechnology have facilitated the co-encapsulation of dyes and drugs within unified drug delivery systems via noncovalent interactions, allowing in vitro and in vivo tracking of therapeutic agents[158]. Notably, Yin and co-workers developed core–shell fluorescent macromolecules, including PDI-cored star polymers and dendrimers, which exhibit high fluorescence quantum yields, excellent photostability, and good biocompatibility, enabling imaging-guided cancer chemotherapy[159]. To address premature drug leakage, stimulus-responsive dye–drug conjugates have also been explored[160,161]. For example, Kim et al. linked fluorophores such as coumarin [162,163], naphthalimide [158], and Cy7 [164] to chemotherapeutic agents via disulfide bonds, allowing glutathione-triggered drug release accompanied by fluorescence changes. Beyond carrier systems, planar aromatic dyes can function as DNA-intercalating agents through rational molecular design. Such intercalators disrupt DNA replication by inserting between base pairs; representative examples include naphthalimide-based polyintercalators with GC-selective binding and perylene bisimide derivatives that combine potent anticancer activity with effective nuclear imaging [165,166].

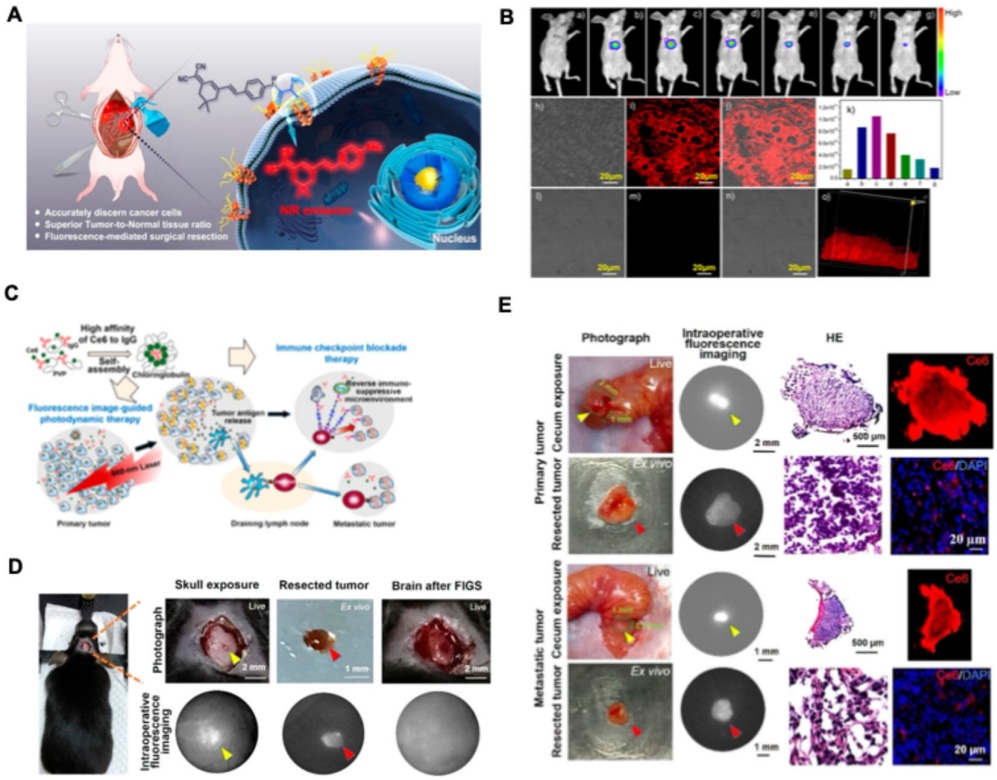

Figure 12. (A) Schematic illustrating the APN recognition and activation mechanism of the probe YH-APN and its biological applications. (B) Imaging of endogenous APN activity in BALB/c mice bearing HepG-2 xenograft

 doi:10.20944/preprints202602.0438.v1

tumors and in normal tissues. Time-dependent fluorescence images after intratumoral injection of YH-APN (50 μM, 50 μL): (a) 0 min, (b) 20 min, (c) 50 min, (d) 70 min, (e) 100 min, (f) 120 min, and (g) 150 min. (k) Corresponding average photon flux (ph/s) from the tumor region. (h–j) Tumor tissue imaging and (l–n) normal tissue imaging. λ_ex = 488 nm, λ_em = 655–755 nm. Scale bar = 20 μm. Whole-body fluorescence imaging was performed using a 475 nm excitation filter (FWHM 20 nm) and a 655 nm emission filter (FWHM 20 nm). (o) Three-dimensional tumor imaging using two-photon excitation at 800 nm and emission at 575–630 nm. Reproduced with permission from [155]. Copyright 2020, American Chemical Society. (C) Chlorin e6–immunoglobulin G conjugate for intraoperative fluorescence image-guided photodynamic therapy (FIG-PDT) combined with immune checkpoint blockade. (D) Fluorescence image-guided surgery (FIGS) of glioma in mice 1 h after i.v. injection of αPD-L1 Chloringlobulin. Top: photographs; bottom: intraoperative fluorescence images showing the exposed skull before craniotomy, resected tumor, and brain after FIGS. Arrowheads indicate tumors with high fluorescence intensity. (E) Intraoperative FIG-PDT of orthotopic CT26-Luc colon tumors 1 h after i.v. injection of αPD-L1–αCTLA-4 Chloringlobulin. Left columns: intraoperative photographs and fluorescence images of exposed cecum with primary or metastatic tumors and resected tumors. Arrowheads indicate high-fluorescence tumor regions. Right columns: H&E staining and corresponding fluorescence images of resected tumors. Reproduced with permission from [157]. Copyright 2019, American Chemical Society.

9. Summary and Outlook

The rapid evolution of optical technologies has profoundly expanded the role of organic dyes in biomedicine, transforming them from conventional fluorescent probes into multifunctional platforms for imaging-guided diagnosis and therapy. Through rational molecular design and chemical modification, organic dyes can be engineered to exhibit diverse light-responsive behaviors, including fluorescence emission, photothermal heat generation, and photodynamic reactive oxygen species production. These tunable photophysical properties, combined with their structural flexibility, have enabled organic dyes to support a wide range of health-related applications extending well beyond traditional bioimaging, such as intraoperative guidance, antimicrobial therapy, cancer treatment, and multimodal theranostics.

Recent advances highlight two major drivers of progress in this field. First, precise regulation of energy conversion pathways through molecular engineering allows a single chromophore scaffold to be adapted for fluorescence imaging, photothermal therapy (PTT), or photodynamic therapy (PDT). Second, application-oriented synthetic strategies—often coupled with polymer chemistry, supramolecular assembly, or nanotechnology—have facilitated the translation of dye-based materials into diagnostic and therapeutic systems with enhanced performance in complex biological environments. Collectively, these developments underscore the versatility of organic dyes as customizable, light-activated agents for integrated biomedical imaging and therapy.

Despite these advances, several critical challenges must be addressed to fully unlock the clinical potential of organic dyes. Stability remains one of the most pressing issues, particularly under prolonged laser irradiation, elevated temperatures, and physiologically harsh conditions. From a synthetic chemistry perspective, increasing molecular rigidity within conjugated backbones—such as introducing fused or six-membered ring structures—has proven effective in suppressing photobleaching and improving thermal robustness. Fused aromatic systems, including rylene-based dyes, further exemplify promising design strategies for achieving long-term photostability without sacrificing optical performance.

Another important future direction lies in the fine regulation of photophysical efficiency, including photothermal conversion efficiency and singlet oxygen ($^1O_2$) quantum yield. While significant progress has been made, achieving consistently high energy conversion remains challenging. Molecular approaches that promote nonradiative decay—such as enhancing intramolecular rotation or facilitating supramolecular radical formation—have demonstrated remarkable improvements in photothermal performance. Similarly, strategic control over intersystem crossing through heavy-atom effects or molecular symmetry disruption offers routes to enhance photodynamic efficacy. As emerging therapeutic paradigms such as sonodynamic and

 doi:10.20944/preprints202602.0438.v1

chemodynamic therapies continue to evolve, organic dyes capable of participating in alternative or hybrid energy conversion pathways are expected to open new therapeutic opportunities.

For in vivo imaging, minimizing biological background interference remains a central design principle. Beyond extending fluorescence emission into the NIR-II window, future efforts will increasingly focus on lifetime-based and persistence-based imaging strategies. Phosphorescent and long-lived emissive dyes enable fluorescence lifetime imaging and time-gated detection, providing improved contrast and deeper tissue visualization. Precise control over both emission wavelength and excited-state lifetime will therefore be a key aspect of next-generation dye design.

Finally, the integration of organic dyes with nanotechnology and smart materials represents a powerful avenue for future development. Chemical modification of chromophores, combined with functional polymer shells or responsive nanostructures, enables the construction of ultrasmall nanoparticles and intelligent delivery systems with enhanced circulation, targeting, and stimulus-responsive behavior. Such hybrid platforms will not only improve imaging sensitivity and therapeutic precision but also accelerate the translation of organic dye-based systems toward clinically relevant, minimally invasive biomedical applications.

n summary, continued advances in molecular design, photophysical regulation, and nanotechnological integration will position organic dyes as cornerstone materials for next-generation light-based biomedical imaging and therapy. Addressing stability, efficiency, and biological specificity in parallel will be essential for moving these versatile systems from proof-of-concept studies toward real-world clinical impact.

Funding: This research received no external funding.

Institutional Review Board Statement: Not applicable.

Informed Consent Statement: Not applicable.

Data Availability Statement: No new data were created or analyzed in this study.

Acknowledgments: P.P.P.K. shows sincere gratitude to the Department of Biomedical Engineering, Micigan State university, for the facilities and use of resources for the literature collections.

Conflicts of Interest: The author declares no conflict of interest.

References

1. Baldini, F.; Dholakia, K.; French, P.; Guntinas-Lichius, O.; Kohler, A.; Mäntele, W.; Marcu, L.; Sroka, R.; Umapathy, S.; Popp, J. Shining a Light on the Future of Biophotonics. *J. Biophotonics* **2025**, *18*, e202500148, doi:10.1002/jbio.202500148.
2. Banstola, A.; Lin, Z.-T.; Li, Y.; Wu, M.X. PhotoChem Interplays: Lighting the Way for Drug Delivery and Diagnosis. *Adv. Drug Deliv. Rev.* **2025**, *219*, 115549, doi:10.1016/j.addr.2025.115549.
3. Datta, R.; Heaster, T.M.; Sharick, J.T.; Gillette, A.A.; Skala, M.C. Fluorescence Lifetime Imaging Microscopy: Fundamentals and Advances in Instrumentation, Analysis, and Applications. *J. Biomed. Opt.* **2020**, *25*, 1, doi:10.1117/1.JBO.25.7.071203.
4. Choi, W.; Park, B.; Choi, S.; Oh, D.; Kim, J.; Kim, C. Recent Advances in Contrast-Enhanced Photoacoustic Imaging: Overcoming the Physical and Practical Challenges. *Chem. Rev.* **2023**, *123*, 7379–7419, doi:10.1021/acs.chemrev.2c00627.
5. Pan, W.; Rafiq, M.; Haider, W.; Guo, Y.; Wang, H.; Xu, M.; Yu, B.; Cong, H.; Shen, Y. Recent Advances in NIR-II Fluorescence/Photoacoustic Dual-Modality Imaging Probes. *Coord. Chem. Rev.* **2024**, *514*, 215907, doi:10.1016/j.ccr.2024.215907.
6. Cuadrado, C.F.; Lagos, K.J.; Stringasci, M.D.; Bagnato, V.S.; Romero, M.P. Clinical and Pre-Clinical Advances in the PDT/PTT Strategy for Diagnosis and Treatment of Cancer. *Photodiagnosis Photodyn Ther.* **2024**, *50*, 104387, doi:10.1016/j.pdpdt.2024.104387.
7. Omidian, H.; Dey Chowdhury, S. Advances in Photothermal and Photodynamic Nanotheranostics for Precision Cancer Treatment. *J. Nanotheranostics* **2024**, *5*, 228–252, doi:10.3390/jnt5040014.

 doi:10.20944/preprints202602.0438.v1

8. Cai, Y.; Chai, T.; Nguyen, W.; Liu, J.; Xiao, E.; Ran, X.; Ran, Y.; Du, D.; Chen, W.; Chen, X. Phototherapy in Cancer Treatment: Strategies and Challenges. *Sig. Transduct. Target. Ther.* **2025**, *10*, 115, doi:10.1038/s41392-025-02140-y.
9. Huis In 'T Veld, R.V.; Heuts, J.; Ma, S.; Cruz, L.J.; Ossendorp, F.A.; Jager, M.J. Current Challenges and Opportunities of Photodynamic Therapy against Cancer. *Pharmaceutics* **2023**, *15*, 330, doi:10.3390/pharmaceutics15020330.
10. Stenspil, S.G.; Laursen, B.W. Photophysics of Fluorescent Nanoparticles Based on Organic Dyes – Challenges and Design Principles. *Chem. Sci.* **2024**, *15*, 8625–8638, doi:10.1039/D4SC01352B.
11. Ostroverkhova, O. Organic Optoelectronic Materials: Mechanisms and Applications. *Chem. Rev.* **2016**, *116*, 13279–13412, doi:10.1021/acs.chemrev.6b00127.
12. Bouachrine, M.; Ayachi, S. Organic Electronics: Pioneering the Future of Sustainable and Flexible Technology. *RSC Adv.* **2025**, *15*, 45177–45195, doi:10.1039/D5RA04656D.
13. Cheng, W.; Chen, H.; Liu, C.; Ji, C.; Ma, G.; Yin, M. Functional Organic Dyes for Health-related Applications. *VIEW* **2020**, *1*, 20200055, doi:10.1002/VIW.20200055.
14. Kumar, P.P.P.; Saxena, S.; Joshi, R. BODIPY Dyes: A New Frontier in Cellular Imaging and Theragnostic Applications. *Colorants* **2025**, *4*, 13, doi:10.3390/colorants4020013.
15. Kumar, P.P.P. The Role of Perylene Diimide Dyes as Cellular Imaging Agents and for Enhancing Phototherapy Outcomes. *Colorants* **2025**, *4*, 22, doi:10.3390/colorants4030022.
16. Jiang, Z.; Ding, Y.; Lovell, J.F.; Zhang, Y. Design and Application of Organic Contrast Agents for Molecular Imaging in the Second near Infrared (NIR-II) Window. *Photoacoustics* **2022**, *28*, 100426, doi:10.1016/j.pacs.2022.100426.
17. Zhao, M.; Chen, X. Recent Advances in NIR-II Materials for Biomedical Applications. *Acc. Mater. Res.* **2024**, *5*, 600–613, doi:10.1021/accountsmr.4c00025.
18. Han, S.; Lee, D.; Kim, S.; Kim, H.-H.; Jeong, S.; Kim, J. Contrast Agents for Photoacoustic Imaging: A Review Focusing on the Wavelength Range. *Biosensors* **2022**, *12*, 594, doi:10.3390/bios12080594.
19. Li, C.; Liu, C.; Fan, Y.; Ma, X.; Zhan, Y.; Lu, X.; Sun, Y. Recent Development of Near-Infrared Photoacoustic Probes Based on Small-Molecule Organic Dye. *RSC Chem. Biol.* **2021**, *2*, 743–758, doi:10.1039/D0CB00225A.
20. Liu, H.; Wang, M.; Ji, F.; Jiang, Y.; Yang, M. Mini Review of Photoacoustic Clinical Imaging: A Noninvasive Tool for Disease Diagnosis and Treatment Evaluation. *J. Biomed. Opt.* **2024**, *29*, doi:10.1117/1.JBO.29.S1.S11522.
21. Goloviznina, K.; Lepre, L.F.; Sabelle, S.; Pádua, A.A.H.; Costa Gomes, M. Enhancement of the Solubility of Organic Dyes in Aqueous Ionic Solvents Doped with Surfactants. *Journal of Molecular Liquids* **2022**, *357*, 118958, doi:10.1016/j.molliq.2022.118958.
22. Kim, J.Y.; Hwang, T.G.; Woo, S.W.; Lee, J.M.; Namgoong, J.W.; Yuk, S.B.; Chung, S.; Kim, J.P. Simple Modification of Basic Dyes with Bulky & Symmetric WCAs for Improving Their Solubilities in Organic Solvents without Color Change. *Sci Rep* **2017**, *7*, 46178, doi:10.1038/srep46178.
23. Svechkarev, D.; Mohs, A.M. Organic Fluorescent Dye-Based Nanomaterials: Advances in the Rational Design for Imaging and Sensing Applications. *Curr. Med. chem.* **2019**, *26*, 4042–4064, doi:10.2174/0929867325666180226111716.
24. Arunkumar, E.; Forbes, C.C.; Smith, B.D. Improving the Properties of Organic Dyes by Molecular Encapsulation. *Eur. J. Org. Chem.* **2005**, *2005*, 4051–4059, doi:10.1002/ejoc.200500372.
25. Li, Y.; Cai, Z.; Liu, S.; Zhang, H.; Wong, S.T.H.; Lam, J.W.Y.; Kwok, R.T.K.; Qian, J.; Tang, B.Z. Design of AIEgens for Near-Infrared IIb Imaging through Structural Modulation at Molecular and Morphological Levels. *Nat. Commun.* **2020**, *11*, 1255, doi:10.1038/s41467-020-15095-1.
26. Cappello, D.; Buguis, F.L.; Gilroy, J.B. Tuning the Properties of Donor–Acceptor and Acceptor–Donor–Acceptor Boron Difluoride Hydrazones *via* Extended π-Conjugation. *ACS Omega* **2022**, *7*, 32727–32739, doi:10.1021/acsomega.2c04401.
27. Ramezani, P.; De Smedt, S.C.; Sauvage, F. Supramolecular Dye Nanoassemblies for Advanced Diagnostics and Therapies. *Bioeng. Transl. Med.* **2024**, *9*, e10652, doi:10.1002/btm2.10652.

 doi:10.20944/preprints202602.0438.v1

28. Zhang, Y.; Yang, Z.; Zheng, X.; Yang, L.; Song, N.; Zhang, L.; Chen, L.; Xie, Z. Heavy Atom Substituted Near-Infrared BODIPY Nanoparticles for Photodynamic Therapy. *Dyes and Pigments* **2020**, *178*, 108348, doi:10.1016/j.dyepig.2020.108348.
29. Kumar, P.P.P.; Yadav, P.; Shanavas, A.; Neelakandan, P.P. Aggregation Enhances Luminescence and Photosensitization Properties of a Hexaiodo-BODIPY. *Mater. Chem. Front.* **2020**, *4*, 965–972, doi:10.1039/D0QM00010H.
30. Fang, L.; Chen, Z.; Dai, J.; Pan, Y.; Tu, Y.; Meng, Q.; Diao, Y.; Yang, S.; Guo, W.; Li, L.; et al. Recent Advances in Strategies to Enhance Photodynamic and Photothermal Therapy Performance of Single-Component Organic Phototherapeutic Agents. *Adv. Sci.* **2025**, *12*, 2409157, doi:10.1002/advs.202409157.
31. Shan, G.; Weissleder, R.; Hilderbrand, S.A. Upconverting Organic Dye Doped Core-Shell Nano-Composites for Dual-Modality NIR Imaging and Photo-Thermal Therapy. *Theranostics* **2013**, *3*, 267–274, doi:10.7150/thno.5226.
32. Reisch, A.; Runser, A.; Arntz, Y.; Mély, Y.; Klymchenko, A.S. Charge-Controlled Nanoprecipitation as a Modular Approach to Ultrasmall Polymer Nanocarriers: Making Bright and Stable Nanoparticles. *ACS Nano* **2015**, *9*, 5104–5116, doi:10.1021/acsnano.5b00214.
33. Sun, X.; Xiang, T.; Xie, L.; Ren, Q.; Chang, J.; Jiang, W.; Jin, Z.; Yang, X.; Ren, W.; Yu, Y. Recent Advances in Fluorescent Nanomaterials Designed for Biomarker Detection and Imaging. *Materials Today Bio* **2025**, *32*, 101763, doi:10.1016/j.mtbio.2025.101763.
34. Nath, P.; Mahtaba, K.R.; Ray, A. Fluorescence-Based Portable Assays for Detection of Biological and Chemical Analytes. *Sensors* **2023**, *23*, 5053, doi:10.3390/s23115053.
35. Spagnolo, A.M. Bacterial Infections: Surveillance, Prevention and Control. *Pathogens* **2024**, *13*, 181, doi:10.3390/pathogens13020181.
36. Tang, X.; Qi, Q.; Li, B.; Zhu, Z.; Lu, J.; Liu, L. Recent Advances on Fluorescent Sensors for Detection of Pathogenic Bacteria. *Chemosensors* **2025**, *13*, 182, doi:10.3390/chemosensors13050182.
37. Salam, Md.A.; Al-Amin, Md.Y.; Pawar, J.S.; Akhter, N.; Lucy, I.B. Conventional Methods and Future Trends in Antimicrobial Susceptibility Testing. *Saudi J. Biol. Sci.* **2023**, *30*, 103582, doi:10.1016/j.sjbs.2023.103582.
38. Boehle, K.E.; Gilliland, J.; Wheeldon, C.R.; Holder, A.; Adkins, J.A.; Geiss, B.J.; Ryan, E.P.; Henry, C.S. Utilizing Paper-Based Devices for Antimicrobial-Resistant Bacteria Detection. *Angew. Chem. Int. Ed.* **2017**, *56*, 6886–6890, doi:10.1002/anie.201702776.
39. Chen, S.; Chen, Q.; Li, Q.; An, J.; Sun, P.; Ma, J.; Gao, H. Biodegradable Synthetic Antimicrobial with Aggregation-Induced Emissive Luminogens for Temporal Antibacterial Activity and Facile Bacteria Detection. *Chem. Mater.* **2018**, *30*, 1782–1790, doi:10.1021/acs.chemmater.8b00251.
40. Wang, W.; Wu, F.; Zhang, Q.; Zhou, N.; Zhang, M.; Zheng, T.; Li, Y.; Tang, B.Z. Aggregation-Induced Emission Nanoparticles for Single Near-Infrared Light-Triggered Photodynamic and Photothermal Antibacterial Therapy. *ACS Nano* **2022**, *16*, 7961–7970, doi:10.1021/acsnano.2c00734.
41. Yang, Y.; He, P.; Wang, Y.; Bai, H.; Wang, S.; Xu, J.; Zhang, X. Supramolecular Radical Anions Triggered by Bacteria In Situ for Selective Photothermal Therapy. *Angew. Chem. Int. Ed.* **2017**, *56*, 16239–16242, doi:10.1002/anie.201708971.
42. Bodaghi, A.; Fattahi, N.; Ramazani, A. Biomarkers: Promising and Valuable Tools towards Diagnosis, Prognosis and Treatment of Covid-19 and Other Diseases. *Heliyon* **2023**, *9*, e13323, doi:10.1016/j.heliyon.2023.e13323.
43. Das, S.; Dey, M.K.; Devireddy, R.; Gartia, M.R. Biomarkers in Cancer Detection, Diagnosis, and Prognosis. *Sensors* **2023**, *24*, 37, doi:10.3390/s24010037.
44. Asci Erkocyigit, B.; Ozufuklar, O.; Yardim, A.; Guler Celik, E.; Timur, S. Biomarker Detection in Early Diagnosis of Cancer: Recent Achievements in Point-of-Care Devices Based on Paper Microfluidics. *Biosensors* **2023**, *13*, 387, doi:10.3390/bios13030387.
45. Wang, Y.; Pei, H.; Jia, Y.; Liu, J.; Li, Z.; Ai, K.; Lu, Z.; Lu, L. Synergistic Tailoring of Electrostatic and Hydrophobic Interactions for Rapid and Specific Recognition of Lysophosphatidic Acid, an Early-Stage Ovarian Cancer Biomarker. *J. Am. Chem. Soc.* **2017**, *139*, 11616–11621, doi:10.1021/jacs.7b06885.

 doi:10.20944/preprints202602.0438.v1

46. Joh, D.Y.; Hucknall, A.M.; Wei, Q.; Mason, K.A.; Lund, M.L.; Fontes, C.M.; Hill, R.T.; Blair, R.; Zimmers, Z.; Achar, R.K.; et al. Inkjet-Printed Point-of-Care Immunoassay on a Nanoscale Polymer Brush Enables Subpicomolar Detection of Analytes in Blood. *Proc. Natl. Acad. Sci. U.S.A.* **2017**, *114*, doi:10.1073/pnas.1703200114.
47. Yang, S.K.; Shi, X.; Park, S.; Doganay, S.; Ha, T.; Zimmerman, S.C. Monovalent, Clickable, Uncharged, Water-Soluble Perylenediimide-Cored Dendrimers for Target-Specific Fluorescent Biolabeling. *J. Am. Chem. Soc.* **2011**, *133*, 9964–9967, doi:10.1021/ja2009136.
48. Zhou, J.; Zhang, J.; Lai, Y.; Zhou, Z.; Zhao, Y.; Wang, H.; Wang, Z. Guanidinium-Dendronized Perylene Bisimides as Stable, Water-Soluble Fluorophores for Live-Cell Imaging. *New J. Chem.* **2013**, *37*, 2983, doi:10.1039/c3nj00876b.
49. Kaur, P.; Singh, K. Recent Advances in the Application of BODIPY in Bioimaging and Chemosensing. *J. Mater. Chem. C* **2019**, *7*, 11361–11405, doi:10.1039/C9TC03719E.
50. Collot, M.; Boutant, E.; Lehmann, M.; Klymchenko, A.S. BODIPY with Tuned Amphiphilicity as a Fluorogenic Plasma Membrane Probe. *Bioconjugate Chem.* **2019**, *30*, 192–199, doi:10.1021/acs.bioconjchem.8b00828.
51. Polita, A.; Stancikaitė, M.; Žvirblis, R.; Maleckaitė, K.; Dodonova-Vaitkūnienė, J.; Tumkevičius, S.; Shivabalan, A.P.; Valinčius, G. Designing a Green-Emitting Viscosity-Sensitive 4,4-Difluoro-4-Bora-3a,4a-Diaza- *s* -Indacene (BODIPY) Probe for Plasma Membrane Viscosity Imaging. *RSC Adv.* **2023**, *13*, 19257–19264, doi:10.1039/D3RA04126C.
52. Li, A.; Wang, F.; Li, Y.; Peng, X.; Liu, Y.; Zhu, L.; He, P.; Yu, T.; Chen, D.; Duan, M.; et al. Fluorination of Aza-BODIPY for Cancer Cell Plasma Membrane-Targeted Imaging and Therapy. *ACS Appl. Mater. Interfaces* **2025**, acsami.4c17943, doi:10.1021/acsami.4c17943.
53. Xiong, T.; Chen, Y.; Peng, Q.; Li, M.; Lu, S.; Chen, X.; Fan, J.; Wang, L.; Peng, X. Pyrazolone-Protein Interaction Enables Long-Term Retention Staining and Facile Artificial Biorecognition on Cell Membranes. *J. Am. Chem. Soc.* **2024**, *146*, 24158–24166, doi:10.1021/jacs.4c08987.
54. Ni, Y.; Zeng, L.; Kang, N.; Huang, K.; Wang, L.; Zeng, Z.; Chang, Y.; Wu, J. *Meso* -Ester and Carboxylic Acid Substituted BODIPYs with Far-Red and Near-Infrared Emission for Bioimaging Applications. *Chemistry A European J* **2014**, *20*, 2301–2310, doi:10.1002/chem.201303868.
55. Jiang, X.-D.; Gao, R.; Yue, Y.; Sun, G.-T.; Zhao, W. A NIR BODIPY Dye Bearing 3,4,4a-Trihydroxanthene Moieties. *Org. Biomol. Chem.* **2012**, *10*, 6861, doi:10.1039/c2ob26218e.
56. Kand, D.; Liu, P.; Navarro, M.X.; Fischer, L.J.; Rousso-Noori, L.; Friedmann-Morvinski, D.; Winter, A.H.; Miller, E.W.; Weinstain, R. Water-Soluble BODIPY Photocages with Tunable Cellular Localization. *J. Am. Chem. Soc.* **2020**, *142*, 4970–4974, doi:10.1021/jacs.9b13219.
57. Zhang, X.; Wu, Y.; Chen, L.; Song, J.; Yang, H. Optical and Photoacoustic Imaging *In Vivo* : Opportunities and Challenges. *Chem. biomed. Imaging* **2023**, *1*, 99–109, doi:10.1021/cbmi.3c00009.
58. Chu, B.; Chen, Z.; Shi, H.; Wu, X.; Wang, H.; Dong, F.; He, Y. Fluorescence, Ultrasonic and Photoacoustic Imaging for Analysis and Diagnosis of Diseases. *Chem. Commun.* **2023**, *59*, 2399–2412, doi:10.1039/D2CC06654H.
59. Asanuma, D.; Sakabe, M.; Kamiya, M.; Yamamoto, K.; Hiratake, J.; Ogawa, M.; Kosaka, N.; Choyke, P.L.; Nagano, T.; Kobayashi, H.; et al. Sensitive β-Galactosidase-Targeting Fluorescence Probe for Visualizing Small Peritoneal Metastatic Tumours in Vivo. *Nat. Commun.* **2015**, *6*, 6463, doi:10.1038/ncomms7463.
60. Hu, D.; Zha, M.; Zheng, H.; Gao, D.; Sheng, Z. Recent Advances in Indocyanine Green-Based Probes for Second Near-Infrared Fluorescence Imaging and Therapy. *Research* **2025**, *8*, 0583, doi:10.34133/research.0583.
61. Gao, Y.; Zhu, L.; Du, Z.; Xiong, J.; Ma, R.; Aili, M.; Alifu, N.; Dong, B. Recent Advances in Near-Infrared Cyanine Dye-Based Fluorescent Nanoprobes for Tumor Imaging and Therapy. *Int. J. Nanotheranostics* **2025**, *Volume 20*, 13911–13937, doi:10.2147/IJN.S542880.
62. Sun, M.; Müllen, K.; Yin, M. Water-Soluble Perylenediimides: Design Concepts and Biological Applications. *Chem. Soc. Rev.* **2016**, *45*, 1513–1528, doi:10.1039/C5CS00754B.
63. Zong, L.; Zhang, H.; Li, Y.; Gong, Y.; Li, D.; Wang, J.; Wang, Z.; Xie, Y.; Han, M.; Peng, Q.; et al. Tunable Aggregation-Induced Emission Nanoparticles by Varying Isolation Groups in Perylene Diimide

 doi:10.20944/preprints202602.0438.v1

Derivatives and Application in Three-Photon Fluorescence Bioimaging. *ACS Nano* **2018**, *12*, 9532–9540, doi:10.1021/acsnano.8b05090.

64. Kulkarni, B.; Malhotra, M.; Jayakannan, M. Perylene-Tagged Polycaprolactone Block Copolymers and Their Enzyme-Biodegradable Fluorescent Nanoassemblies for Intracellular Bio-Imaging in Cancer Cells. *ACS Appl. Polym. Mater.* **2019**, *1*, 3375–3388, doi:10.1021/acsapm.9b00800.
65. Li, Z.; Lin, T.-P.; Liu, S.; Huang, C.-W.; Hudnall, T.W.; Gabbaï, F.P.; Conti, P.S. Rapid Aqueous [18F]-Labeling of a Bodipy Dye for Positron Emission Tomography/Fluorescence Dual Modality Imaging. *Chem. Commun.* **2011**, *47*, 9324, doi:10.1039/c1cc13089g.
66. Chansaenpak, K.; Wang, H.; Wang, M.; Giglio, B.; Ma, X.; Yuan, H.; Hu, S.; Wu, Z.; Li, Z. Synthesis and Evaluation of [^{18} F]-Ammonium BODIPY Dyes as Potential Positron Emission Tomography Agents for Myocardial Perfusion Imaging. *Chem. Eur. J.* **2016**, *22*, 12122–12129, doi:10.1002/chem.201601972.
67. Liu, S.; Lin, T.-P.; Li, D.; Leamer, L.; Shan, H.; Li, Z.; Gabbaï, F.P.; Conti, P.S. Lewis Acid-Assisted Isotopic^{18} F-^{19} F Exchange in BODIPY Dyes: Facile Generation of Positron Emission Tomography/Fluorescence Dual Modality Agents for Tumor Imaging. *Theranostics* **2013**, *3*, 181–189, doi:10.7150/thno.5984.
68. Liu, S.; Li, D.; Zhang, Z.; Surya Prakash, G.K.; Conti, P.S.; Li, Z. Efficient Synthesis of Fluorescent-PET Probes Based on [18F]BODIPY Dye. *Chem. Commun.* **2014**, *50*, 7371, doi:10.1039/c4cc01411a.
69. Leiloglou, M.; Kedrzycki, M.S.; Chalau, V.; Chiarini, N.; Thiruchelvam, P.T.R.; Hadjiminas, D.J.; Hogben, K.R.; Rashid, F.; Ramakrishnan, R.; Darzi, A.W.; et al. Indocyanine Green Fluorescence Image Processing Techniques for Breast Cancer Macroscopic Demarcation. *Sci. Rep.* **2022**, *12*, 8607, doi:10.1038/s41598-022-12504-x.
70. Chen, Y.; Liu, W.; Li, B.; Gao, X.; Zhou, K.; Zhang, M.; Yang, G.; Cui, M. Synthesis, Preclinical Evaluation, and First-in-Human Assessment of ICG-PSMA-D5: A PSMA-Targeted Probe for Fluorescence-Guided Surgery of Prostate Cancer. *J. Med. Chem.* **2025**, *68*, 3858–3872, doi:10.1021/acs.jmedchem.4c02989.
71. Sheng, Z.; Hu, D.; Zheng, M.; Zhao, P.; Liu, H.; Gao, D.; Gong, P.; Gao, G.; Zhang, P.; Ma, Y.; et al. Smart Human Serum Albumin-Indocyanine Green Nanoparticles Generated by Programmed Assembly for Dual-Modal Imaging-Guided Cancer Synergistic Phototherapy. *ACS Nano* **2014**, *8*, 12310–12322, doi:10.1021/nn5062386.
72. Deng, G.; Zhu, T.; Zhou, L.; Zhang, J.; Li, S.; Sun, Z.; Lai, J.; Meng, X.; Li, W.; Zhang, P.; et al. Bovine Serum Albumin-Loaded Nano-Selenium/ICG Nanoparticles for Highly Effective Chemo-Photothermal Combination Therapy. *RSC Adv.* **2017**, *7*, 30717–30724, doi:10.1039/C7RA02384G.
73. Beard, P. Biomedical Photoacoustic Imaging. *Interface Focus.* **2011**, *1*, 602–631, doi:10.1098/rsfs.2011.0028.
74. Jung, D.; Park, S.; Lee, C.; Kim, H. Recent Progress on Near-Infrared Photoacoustic Imaging: Imaging Modality and Organic Semiconducting Agents. *Polymers* **2019**, *11*, 1693, doi:10.3390/polym11101693.
75. Kim, C.; Song, K.H.; Gao, F.; Wang, L.V. Sentinel Lymph Nodes and Lymphatic Vessels: Noninvasive Dual-Modality in Vivo Mapping by Using Indocyanine Green in Rats—Volumetric Spectroscopic Photoacoustic Imaging and Planar Fluorescence Imaging. *Radiology* **2010**, *255*, 442–450, doi:10.1148/radiol.10090281.
76. Sano, K.; Ohashi, M.; Kanazaki, K.; Makino, A.; Ding, N.; Deguchi, J.; Kanada, Y.; Ono, M.; Saji, H. Indocyanine Green-Labeled Polysarcosine for in Vivo Photoacoustic Tumor Imaging. *Bioconjugate Chem.* **2017**, *28*, 1024–1030, doi:10.1021/acs.bioconjchem.6b00715.
77. Capozza, M.; Blasi, F.; Valbusa, G.; Oliva, P.; Cabella, C.; Buonsanti, F.; Cordaro, A.; Pizzuto, L.; Maiocchi, A.; Poggi, L. Photoacoustic Imaging of Integrin-Overexpressing Tumors Using a Novel ICG-Based Contrast Agent in Mice. *Photoacoustics* **2018**, *11*, 36–45, doi:10.1016/j.pacs.2018.07.007.
78. Zhu, K.; Zhang, X.; Wu, Y.; Song, J. Ratiometric Optical and Photoacoustic Imaging *In Vivo* in the Second Near-Infrared Window. *Acc. Chem. Res.* **2023**, *56*, 3223–3234, doi:10.1021/acs.accounts.3c00495.
79. Wang, S.; Yu, G.; Ma, Y.; Yang, Z.; Liu, Y.; Wang, J.; Chen, X. Ratiometric Photoacoustic Nanoprobe for Bioimaging of Cu^{2+}. *ACS Appl. Mater. Interfaces* **2019**, *11*, 1917–1923, doi:10.1021/acsami.8b20113.
80. Li, X.; Tang, Y.; Li, J.; Hu, X.; Yin, C.; Yang, Z.; Wang, Q.; Wu, Z.; Lu, X.; Wang, W.; et al. A Small-Molecule Probe for Ratiometric Photoacoustic Imaging of Hydrogen Sulfide in Living Mice. *Chem. Commun.* **2019**, *55*, 5934–5937, doi:10.1039/C9CC02224D.

 doi:10.20944/preprints202602.0438.v1

81. Rong, X.; Xia, X.; Wang, R.; Su, Z.; Liu, T.; Zhang, Z.; Long, S.; Du, J.; Fan, J.; Sun, W.; et al. Near-Infrared and Highly Photostable Squaraine-Based Nanoparticles for Photoacoustic Imaging Guided Photothermal Therapy. *Dyes and Pigments* **2023**, *211*, 111055, doi:10.1016/j.dyepig.2022.111055.
82. An, F.-F.; Deng, Z.-J.; Ye, J.; Zhang, J.-F.; Yang, Y.-L.; Li, C.-H.; Zheng, C.-J.; Zhang, X.-H. Aggregation-Induced Near-Infrared Absorption of Squaraine Dye in an Albumin Nanocomplex for Photoacoustic Tomography in Vivo. *ACS Appl. Mater. Interfaces* **2014**, *6*, 17985–17992, doi:10.1021/am504816h.
83. Merkes, J.M.; Lammers, T.; Kancherla, R.; Rueping, M.; Kiessling, F.; Banala, S. Tuning Optical Properties of BODIPY Dyes by Pyrrole Conjugation for Photoacoustic Imaging. *Advanced Optical Materials* **2020**, *8*, 1902115, doi:10.1002/adom.201902115.
84. Xiang, P.; Shen, Y.; Shen, J.; Feng, Z.; Sun, M.; Zhang, Q.; Li, S.; Li, D.; Zhang, G.; Wu, Z.; et al. Functional Terpyridyl Iron Complexes for *in Vivo* Photoacoustic Imaging. *Inorg. Chem. Front.* **2020**, *7*, 2753–2758, doi:10.1039/D0QI00058B.
85. Chitgupi, U.; Lovell, J.F. Naphthalocyanines as Contrast Agents for Photoacoustic and Multimodal Imaging. *Biomed. Eng. Lett.* **2018**, *8*, 215–221, doi:10.1007/s13534-018-0059-2.
86. Duffy, M.J.; Planas, O.; Faust, A.; Vogl, T.; Hermann, S.; Schäfers, M.; Nonell, S.; Strassert, C.A. Towards Optimized Naphthalocyanines as Sonochromes for Photoacoustic Imaging in Vivo. *Photoacoustics* **2018**, *9*, 49–61, doi:10.1016/j.pacs.2017.12.001.
87. Zhang, Y.; Jeon, M.; Rich, L.J.; Hong, H.; Geng, J.; Zhang, Y.; Shi, S.; Barnhart, T.E.; Alexandridis, P.; Huizinga, J.D.; et al. Non-Invasive Multimodal Functional Imaging of the Intestine with Frozen Micellar Naphthalocyanines. *Nature Nanotech.* **2014**, *9*, 631–638, doi:10.1038/nnano.2014.130.
88. Lee, C.; Kim, J.; Zhang, Y.; Jeon, M.; Liu, C.; Song, L.; Lovell, J.F.; Kim, C. Dual-Color Photoacoustic Lymph Node Imaging Using Nanoformulated Naphthalocyanines. *Biomaterials* **2015**, *73*, 142–148, doi:10.1016/j.biomaterials.2015.09.023.
89. Zhang, Y.; Hong, H.; Sun, B.; Carter, K.; Qin, Y.; Wei, W.; Wang, D.; Jeon, M.; Geng, J.; Nickles, R.J.; et al. Surfactant-Stripped Naphthalocyanines for Multimodal Tumor Theranostics with Upconversion Guidance Cream. *Nanoscale* **2017**, *9*, 3391–3398, doi:10.1039/C6NR09321C.
90. Choi, H.; Choi, W.; Kim, J.; Kong, W.H.; Kim, K.S.; Kim, C.; Hahn, S.K. Multifunctional Nanodroplets Encapsulating Naphthalocyanine and Perfluorohexane for Bimodal Image-Guided Therapy. *Biomacromolecules* **2019**, *20*, 3767–3777, doi:10.1021/acs.biomac.9b00842.
91. Fan, Q.; Cheng, K.; Yang, Z.; Zhang, R.; Yang, M.; Hu, X.; Ma, X.; Bu, L.; Lu, X.; Xiong, X.; et al. Perylene-Diimide-Based Nanoparticles as Highly Efficient Photoacoustic Agents for Deep Brain Tumor Imaging in Living Mice. *Adv. Mater.* **2015**, *27*, 843–847, doi:10.1002/adma.201402972.
92. Yang, Y.; Fryer, C.; Sharkey, J.; Thomas, A.; Wais, U.; Jackson, A.W.; Wilm, B.; Murray, P.; Zhang, H. Perylene Diimide Nanoprobes for In Vivo Tracking of Mesenchymal Stromal Cells Using Photoacoustic Imaging. *ACS Appl. Mater. Interfaces* **2020**, *12*, 27930–27939, doi:10.1021/acsami.0c03857.
93. Cui, C.; Yang, Z.; Hu, X.; Wu, J.; Shou, K.; Ma, H.; Jian, C.; Zhao, Y.; Qi, B.; Hu, X.; et al. Organic Semiconducting Nanoparticles as Efficient Photoacoustic Agents for Lightening Early Thrombus and Monitoring Thrombolysis in Living Mice. *ACS Nano* **2017**, *11*, 3298–3310, doi:10.1021/acsnano.7b00594.
94. Jokerst, J.V.; Gambhir, S.S. Molecular Imaging with Theranostic Nanoparticles. *Acc. Chem. Res.* **2011**, *44*, 1050–1060, doi:10.1021/ar200106e.
95. Wang, Y.; Yan, B.; Chen, L. SERS Tags: Novel Optical Nanoprobes for Bioanalysis. *Chem. Rev.* **2013**, *113*, 1391–1428, doi:10.1021/cr300120g.
96. Pimenta, S.; Correia, J.H. Biomedical Applications of Raman Spectroscopy: A Review. *Photochem* **2025**, *5*, 29, doi:10.3390/photochem5040029.
97. Kumar, P.P.P.; Kaushal, S.; Lim, D.-K. Recent Advances in Nano/Microfabricated Substrate Platforms and Artificial Intelligence for Practical Surface-Enhanced Raman Scattering-Based Bioanalysis. *Trends Anal. Chem.* **2023**, *168*, 117341, doi:10.1016/j.trac.2023.117341.
98. Wu, M.C.; Wei, J.H.; Fan, R.Y.; Sim, E.Z.; Yong, K.; Gong, T.; Kong, K.V. Self-Assembled BODIPY@Au Core-Shell Structures for Durable Neuroprotective Phototherapy. *ChemBioChem.* **2025**, *26*, e202400562, doi:10.1002/cbic.202400562.

 doi:10.20944/preprints202602.0438.v1

99. Adarsh, N.; Ramya, A.N.; Maiti, K.K.; Ramaiah, D. Unveiling NIR Aza-Boron-Dipyrromethene (BODIPY) Dyes as Raman Probes: Surface-Enhanced Raman Scattering (SERS)-Guided Selective Detection and Imaging of Human Cancer Cells. *Chemistry A European J* **2017**, *23*, 14286–14291, doi:10.1002/chem.201702626.
100. Klapper, M.; Ehmke, M.; Palgunow, D.; Böhme, M.; Matthäus, C.; Bergner, G.; Dietzek, B.; Popp, J.; Döring, F. Fluorescence-Based Fixative and Vital Staining of Lipid Droplets in Caenorhabditis Elegans Reveal Fat Stores Using Microscopy and Flow Cytometry Approaches. *Journal of Lipid Research* **2011**, *52*, 1281–1293, doi:10.1194/jlr.D011940.
101. Lim, D.-K.; Kumar, P.P.P. Recent Advances in SERS-Based Bioanalytical Applications: Live Cell Imaging. *Nanophotonics* **2024**, *13*, 1521–1534, doi:10.1515/nanoph-2023-0362.
102. Kneipp, J.; Kneipp, H.; Rice, W.L.; Kneipp, K. Optical Probes for Biological Applications Based on Surface-Enhanced Raman Scattering from Indocyanine Green on Gold Nanoparticles. *Anal. Chem.* **2005**, *77*, 2381–2385, doi:10.1021/ac050109v.
103. Garnaik, U.; Chandra, A.; Goel, V.; Gulyás, B.; Padmanabhan, P.; Agarwal, S. Development of SERS Active Nanoprobe for Selective Adsorption and Detection of Alzheimer's Disease Biomarkers Based on Molecular Docking. *Int. J Nanomedicine.* **2024**, *Volume 19*, 8271–8284, doi:10.2147/IJN.S446212.
104. Kneipp, J.; Kneipp, H.; Rajadurai, A.; Redmond, R.W.; Kneipp, K. Optical Probing and Imaging of Live Cells Using SERS Labels. *J. Raman Spectroscopy* **2009**, *40*, 1–5, doi:10.1002/jrs.2060.
105. Von Maltzahn, G.; Centrone, A.; Park, J.; Ramanathan, R.; Sailor, M.J.; Hatton, T.A.; Bhatia, S.N. SERS-Coded Gold Nanorods as a Multifunctional Platform for Densely Multiplexed Near-Infrared Imaging and Photothermal Heating. *Adv. Mater.* **2009**, *21*, 3175–3180, doi:10.1002/adma.200803464.
106. Wang, X.; Chen, L.; Wei, J.; Zheng, H.; Zhou, N.; Xu, X.; Deng, X.; Liu, T.; Zou, Y. The Immune System in Cardiovascular Diseases: From Basic Mechanisms to Therapeutic Implications. *Sig Transduct Target Ther.* **2025**, *10*, 166, doi:10.1038/s41392-025-02220-z.
107. Li, B.; Zhao, M.; Feng, L.; Dou, C.; Ding, S.; Zhou, G.; Lu, L.; Zhang, H.; Chen, F.; Li, X.; et al. Organic NIR-II Molecule with Long Blood Half-Life for in Vivo Dynamic Vascular Imaging. *Nat. Commun.* **2020**, *11*, 3102, doi:10.1038/s41467-020-16924-z.
108. Sun, C.; Li, B.; Zhao, M.; Wang, S.; Lei, Z.; Lu, L.; Zhang, H.; Feng, L.; Dou, C.; Yin, D.; et al. *J* -Aggregates of Cyanine Dye for NIR-II *in Vivo* Dynamic Vascular Imaging beyond 1500 Nm. *J. Am. Chem. Soc.* **2019**, *141*, 19221–19225, doi:10.1021/jacs.9b10043.
109. Narita, Y.; Shimizu, K.; Ikemoto, K.; Uchino, R.; Kosugi, M.; Maess, M.B.; Magata, Y.; Oku, N.; Ogawa, M. Macrophage-Targeted, Enzyme-Triggered Fluorescence Switch-on System for Detection of Embolism-Vulnerable Atherosclerotic Plaques. *Journal of Controlled Release* **2019**, *302*, 105–115, doi:10.1016/j.jconrel.2019.03.025.
110. Park, S.-J.; Kim, B.; Choi, S.; Balasubramaniam, S.; Lee, S.-C.; Lee, J.Y.; Kim, H.S.; Kim, J.-Y.; Kim, J.-J.; Lee, Y.-A.; et al. Imaging Inflammation Using an Activated Macrophage Probe with Slc18b1 as the Activation-Selective Gating Target. *Nat. Commun.* **2019**, *10*, 1111, doi:10.1038/s41467-019-08990-9.
111. Li, L.; Chen, Y.; Chen, W.; Tan, Y.; Chen, H.; Yin, J. Photodynamic Therapy Based on Organic Small Molecular Fluorescent Dyes. *Chinese Chemical Letters* **2019**, *30*, 1689–1703, doi:10.1016/j.cclet.2019.04.017.
112. Ain, N.U.; Rehman, Z.; Ibrahim, T.K.; Kebaili, I.; Boukhris, I.; Al-Buriahi, M.S. Organic Dyes-Based Photothermal Ablation of Cancer Cells: A Review. *Dyes and Pigments* **2025**, *237*, 112687, doi:10.1016/j.dyepig.2025.112687.
113. Kejík, Z.; Hajduch, J.; Abramenko, N.; Vellieux, F.; Veselá, K.; Fialová, J.L.; Petrláková, K.; Kučnirová, K.; Kaplánek, R.; Tatar, A.; et al. Cyanine Dyes in the Mitochondria-Targeting Photodynamic and Photothermal Therapy. *Commun. Chem.* **2024**, *7*, 180, doi:10.1038/s42004-024-01256-6.
114. Mok, H.; Jeong, H.; Kim, S.-J.; Chung, B.H. Indocyanine Green Encapsulated Nanogels for Hyaluronidase Activatable and Selective near Infrared Imaging of Tumors and Lymph Nodes. *Chem. Commun.* **2012**, *48*, 8628, doi:10.1039/c2cc33555g.
115. Peng, C.-L.; Shih, Y.-H.; Lee, P.-C.; Hsieh, T.M.-H.; Luo, T.-Y.; Shieh, M.-J. Multimodal Image-Guided Photothermal Therapy Mediated by^{188} Re-Labeled Micelles Containing a Cyanine-Type Photosensitizer. *ACS Nano* **2011**, *5*, 5594–5607, doi:10.1021/nn201100m.

 doi:10.20944/preprints202602.0438.v1

116. Hassan, M.; Su, Y.T.; Iqbal, S.Z.; Nawaz, R.; Wang, Y.; Jiang, W. Symmetrically Fluorinated D-π-A Structured Cyanine Dye for Highly Efficient NIR-II Imaging-Guided Cancer Phototheranostics. *Small* **2024**, *20*, 2401905, doi:10.1002/smll.202401905.
117. Han, H.S.; Choi, K.Y. Advances in Nanomaterial-Mediated Photothermal Cancer Therapies: Toward Clinical Applications. *Biomedicines* **2021**, *9*, 305, doi:10.3390/biomedicines9030305.
118. Bartusik-Aebisher, D.; Rogóż, K.; Henrykowska, G.; Aebisher, D. Advances in Near-Infrared BODIPY Photosensitizers: Design Strategies and Applications in Photodynamic and Photothermal Therapy. *Pharmaceuticals* **2025**, *19*, 53, doi:10.3390/ph19010053.
119. Kim, G.; Luo, Y.; Shin, M.; Bouffard, J.; Bae, J.; Kim, Y. Making the Brightest Ones Dim: Maximizing the Photothermal Conversion Efficiency of BODIPY-Based Photothermal Agents. *Adv Healthcare Materials* **2024**, *13*, 2400885, doi:10.1002/adhm.202400885.
120. Liu, Y.; Song, N.; Chen, L.; Liu, S.; Xie, Z. Synthesis of a Near-Infrared BODIPY Dye for Bioimaging and Photothermal Therapy. *Chemistry An Asian Journal* **2018**, *13*, 989–995, doi:10.1002/asia.201701727.
121. Pewklang, T.; Saiyasombat, W.; Chueakwon, P.; Ouengwanarat, B.; Chansaenpak, K.; Kampaengsri, S.; Lai, R.; Kamkaew, A. Revolutionary Pyrazole-based Aza-BODIPY: Harnessing Photothermal Power Against Cancer Cells and Bacteria. *ChemBioChem* **2024**, *25*, e202300653, doi:10.1002/cbic.202300653.
122. Yang, Z.; Tian, R.; Wu, J.; Fan, Q.; Yung, B.C.; Niu, G.; Jacobson, O.; Wang, Z.; Liu, G.; Yu, G.; et al. Impact of Semiconducting Perylene Diimide Nanoparticle Size on Lymph Node Mapping and Cancer Imaging. *ACS Nano* **2017**, *11*, 4247–4255, doi:10.1021/acsnano.7b01261.
123. Yang, Z.; Fan, W.; Zou, J.; Tang, W.; Li, L.; He, L.; Shen, Z.; Wang, Z.; Jacobson, O.; Aronova, M.A.; et al. Precision Cancer Theranostic Platform by In Situ Polymerization in Perylene Diimide-Hybridized Hollow Mesoporous Organosilica Nanoparticles. *J. Am. Chem. Soc.* **2019**, *141*, 14687–14698, doi:10.1021/jacs.9b06086.
124. Yuan, A.; Wu, J.; Tang, X.; Zhao, L.; Xu, F.; Hu, Y. Application of Near-Infrared Dyes for Tumor Imaging, Photothermal, and Photodynamic Therapies. *Journal of Pharmaceutical Sciences* **2013**, *102*, 6–28, doi:10.1002/jps.23356.
125. Ciubini, B.; Visentin, S.; Serpe, L.; Canaparo, R.; Fin, A.; Barbero, N. Design and Synthesis of Symmetrical Pentamethine Cyanine Dyes as NIR Photosensitizers for PDT. *Dyes and Pigments* **2019**, *160*, 806–813, doi:10.1016/j.dyepig.2018.09.009.
126. Jiao, L.; Song, F.; Cui, J.; Peng, X. A Near-Infrared Heptamethine Aminocyanine Dye with a Long-Lived Excited Triplet State for Photodynamic Therapy. *Chem. Commun.* **2018**, *54*, 9198–9201, doi:10.1039/C8CC04582H.
127. Kim, B.; Sui, B.; Yue, X.; Tang, S.; Tichy, M.G.; Belfield, K.D. In Vitro Photodynamic Studies of a BODIPY-Based Photosensitizer. *Eur J Org Chem* **2017**, *2017*, 25–28, doi:10.1002/ejoc.201601054.
128. Jung, H.S.; Han, J.; Shi, H.; Koo, S.; Singh, H.; Kim, H.-J.; Sessler, J.L.; Lee, J.Y.; Kim, J.-H.; Kim, J.S. Overcoming the Limits of Hypoxia in Photodynamic Therapy: A Carbonic Anhydrase IX-Targeted Approach. *J. Am. Chem. Soc.* **2017**, *139*, 7595–7602, doi:10.1021/jacs.7b02396.
129. Kumar, P.P.P.; Yadav, P.; Shanavas, A.; Thurakkal, S.; Joseph, J.; Neelakandan, P.P. A Three-Component Supramolecular Nanocomposite as a Heavy-Atom-Free Photosensitizer. *Chem. Commun.* **2019**, *55*, 5623–5626, doi:10.1039/C9CC02480H.
130. Rahman, A.; Praveen Kumar, P.P.; Yadav, P.; Goswami, T.; Shanavas, A.; Ghosh, H.N.; Neelakandan, P.P. Gold–BODIPY Nanoparticles with Luminescence and Photosensitization Properties for Photodynamic Therapy and Cell Imaging. *ACS Appl. Nano Mater.* **2022**, *5*, 6532–6542, doi:10.1021/acsanm.2c00616.
131. Kumar, P.P.P. A Multimode Detection Platform for Biothiols Using BODIPY Dye-Conjugated Gold Nanoparticles. *Colorants* **2024**, *3*, 214–228, doi:10.3390/colorants3030015.
132. Praveen Kumar, P.P.; Kaur, N.; Shanavas, A.; Neelakandan, P.P. Nanomolar Detection of Biothiols *via* Turn-ON Fluorescent Indicator Displacement. *Analyst* **2020**, *145*, 851–857, doi:10.1039/C9AN02222H.
133. Chornovolenko, K.; Koczorowski, T. Phthalocyanines Conjugated with Small Biologically Active Compounds for the Advanced Photodynamic Therapy: A Review. *Molecules* **2025**, *30*, 3297, doi:10.3390/molecules30153297.

 doi:10.20944/preprints202602.0438.v1

134. Wang, H.; Wang, S.; Liu, Z.; Dong, C.; Yang, J.; Gong, X.; Chang, J. Upconverting Crystal/Dextran-g-DOPE with High Fluorescence Stability for Simultaneous Photodynamic Therapy and Cell Imaging. *Nanotechnology* **2014**, *25*, 155103, doi:10.1088/0957-4484/25/15/155103.
135. Avşar, G.; Sari, F.A.; Yuzer, A.C.; Soylu, H.M.; Er, O.; Ince, M.; Lambrecht, F.Y. Intracellular Uptake and Fluorescence Imaging Potential in Tumor Cell of Zinc Phthalocyanine. *International Journal of Pharmaceutics* **2016**, *505*, 369–375, doi:10.1016/j.ijpharm.2016.04.023.
136. Zhao, Z.; Chan, P.-S.; Li, H.; Wong, K.-L.; Wong, R.N.S.; Mak, N.-K.; Zhang, J.; Tam, H.-L.; Wong, W.-Y.; Kwong, D.W.J.; et al. Highly Selective Mitochondria-Targeting Amphiphilic Silicon(IV) Phthalocyanines with Axially Ligated Rhodamine B for Photodynamic Therapy. *Inorg. Chem.* **2012**, *51*, 812–821, doi:10.1021/ic201178e.
137. Li, K.; Qiu, L.; Liu, Q.; Lv, G.; Zhao, X.; Wang, S.; Lin, J. Conjugate of Biotin with Silicon(IV) Phthalocyanine for Tumor-Targeting Photodynamic Therapy. *Journal of Photochemistry and Photobiology B: Biology* **2017**, *174*, 243–250, doi:10.1016/j.jphotobiol.2017.08.003.
138. Zheng, B.-Y.; Yang, X.-Q.; Zhao, Y.; Zheng, Q.-F.; Ke, M.-R.; Lin, T.; Chen, R.-X.; Ho, K.K.K.; Kumar, N.; Huang, J.-D. Synthesis and Photodynamic Activities of Integrin-Targeting Silicon(IV) Phthalocyanine-cRGD Conjugates. *European Journal of Medicinal Chemistry* **2018**, *155*, 24–33, doi:10.1016/j.ejmech.2018.05.039.
139. Hill, J.E.; Linder, M.K.; Davies, K.S.; Sawada, G.A.; Morgan, J.; Ohulchanskyy, T.Y.; Detty, M.R. Selenorhodamine Photosensitizers for Photodynamic Therapy of P-Glycoprotein-Expressing Cancer Cells. *J. Med. Chem.* **2014**, *57*, 8622–8634, doi:10.1021/jm501259v.
140. Caldas, M.; Artiga, Á.; Marin, R.; Ming, L.; Jaque, D.; Silva, L.P.D.; Reis, R.L.; Correlo, V.M. Enhanced Cell Uptake of Rhodamine B for Photodynamic Therapy under Hypoxic Conditions Using Sepia Melanin Nanoparticles. *ACS Appl. Nano Mater.* **2025**, *8*, 16328–16339, doi:10.1021/acsanm.5c02567.
141. Piao, W.; Hanaoka, K.; Fujisawa, T.; Takeuchi, S.; Komatsu, T.; Ueno, T.; Terai, T.; Tahara, T.; Nagano, T.; Urano, Y. Development of an Azo-Based Photosensitizer Activated under Mild Hypoxia for Photodynamic Therapy. *J. Am. Chem. Soc.* **2017**, *139*, 13713–13719, doi:10.1021/jacs.7b05019.
142. Chiba, M.; Ichikawa, Y.; Kamiya, M.; Komatsu, T.; Ueno, T.; Hanaoka, K.; Nagano, T.; Lange, N.; Urano, Y. An Activatable Photosensitizer Targeted to γ-Glutamyltranspeptidase. *Angew Chem Int Ed* **2017**, *56*, 10418–10422, doi:10.1002/anie.201704793.
143. Wang, Z.; Liu, X.; Ma, Y.; Zheng, J.; Xu, K.; Chang, Y.; Ye, Z.; Ling, Y.; Wang, L. Novel Type I/II Carbazole/Benzindole Photosensitizers Achieve Chemo-Photodynamic Synergistic Therapy for Suppressing Solid Tumors and Drug-Resistant Bacterial Infections. *Molecules* **2025**, *30*, 2560, doi:10.3390/molecules30122560.
144. Zhang, C.-J.; Hu, Q.; Feng, G.; Zhang, R.; Yuan, Y.; Lu, X.; Liu, B. Image-Guided Combination Chemotherapy and Photodynamic Therapy Using a Mitochondria-Targeted Molecular Probe with Aggregation-Induced Emission Characteristics. *Chem. Sci.* **2015**, *6*, 4580–4586, doi:10.1039/C5SC00826C.
145. Yuan, Y.; Zhang, C.-J.; Xu, S.; Liu, B. A Self-Reporting AIE Probe with a Built-in Singlet Oxygen Sensor for Targeted Photodynamic Ablation of Cancer Cells. *Chem. Sci.* **2016**, *7*, 1862–1866, doi:10.1039/C5SC03583J.
146. Wang, D.; Su, H.; Kwok, R.T.K.; Hu, X.; Zou, H.; Luo, Q.; Lee, M.M.S.; Xu, W.; Lam, J.W.Y.; Tang, B.Z. Rational Design of a Water-Soluble NIR AIEgen, and Its Application in Ultrafast Wash-Free Cellular Imaging and Photodynamic Cancer Cell Ablation. *Chem. Sci.* **2018**, *9*, 3685–3693, doi:10.1039/C7SC04963C.
147. Zou, J.; Lu, H.; Zhao, X.; Li, W.; Guan, Y.; Zheng, Y.; Zhang, L.; Gao, H. A Multi-Functional Fluorescent Probe with Aggregation-Induced Emission Characteristics: Mitochondrial Imaging, Photodynamic Therapy and Visualizing Therapeutic Process in Zebrafish Model. *Dyes and Pigments* **2018**, *151*, 45–53, doi:10.1016/j.dyepig.2017.12.044.
148. Hu, W.; Xie, M.; Zhao, H.; Tang, Y.; Yao, S.; He, T.; Ye, C.; Wang, Q.; Lu, X.; Huang, W.; et al. Nitric Oxide Activatable Photosensitizer Accompanying Extremely Elevated Two-Photon Absorption for Efficient Fluorescence Imaging and Photodynamic Therapy. *Chem. Sci.* **2018**, *9*, 999–1005, doi:10.1039/C7SC04044J.
149. Zheng, Z.; Zhang, T.; Liu, H.; Chen, Y.; Kwok, R.T.K.; Ma, C.; Zhang, P.; Sung, H.H.Y.; Williams, I.D.; Lam, J.W.Y.; et al. Bright Near-Infrared Aggregation-Induced Emission Luminogens with Strong Two-Photon Absorption, Excellent Organelle Specificity, and Efficient Photodynamic Therapy Potential. *ACS Nano* **2018**, *12*, 8145–8159, doi:10.1021/acsnano.8b03138.

 doi:10.20944/preprints202602.0438.v1

150. Liu, Y.; Hu, X.; Wang, L.; Liu, X.; Bing, T.; Tan, W.; Shangguan, D. Quinacridone Derivative as a New Photosensitizer: Photodynamic Effects in Cells and in Vivo. *Dyes and Pigments* **2017**, *145*, 168–173, doi:10.1016/j.dyepig.2017.06.003.
151. Li, M.; Xia, J.; Tian, R.; Wang, J.; Fan, J.; Du, J.; Long, S.; Song, X.; Foley, J.W.; Peng, X. Near-Infrared Light-Initiated Molecular Superoxide Radical Generator: Rejuvenating Photodynamic Therapy against Hypoxic Tumors. *J. Am. Chem. Soc.* **2018**, *140*, 14851–14859, doi:10.1021/jacs.8b08658.
152. Wang, R.; Hua, S.; Xing, Y.; Wang, R.; Wang, H.; Jiang, T.; Yu, F. Organic Dye-Based Photosensitizers for Fluorescence Imaging-Guided Cancer Phototheranostics. *Coordination Chemistry Reviews* **2024**, *513*, 215866, doi:10.1016/j.ccr.2024.215866.
153. Rainu, S.K.; Ramachandran, R.G.; Parameswaran, S.; Krishnakumar, S.; Singh, N. Advancements in Intraoperative Near-Infrared Fluorescence Imaging for Accurate Tumor Resection: A Promising Technique for Improved Surgical Outcomes and Patient Survival. *ACS Biomater. Sci. Eng.* **2023**, *9*, 5504–5526, doi:10.1021/acsbiomaterials.3c00828.
154. Li, S.; Cheng, D.; He, L.; Yuan, L. Recent Progresses in NIR-I/II Fluorescence Imaging for Surgical Navigation. *Front. Bioeng. Biotechnol.* **2021**, *9*, 768698, doi:10.3389/fbioe.2021.768698.
155. Li, H.; Yao, Q.; Sun, W.; Shao, K.; Lu, Y.; Chung, J.; Kim, D.; Fan, J.; Long, S.; Du, J.; et al. Aminopeptidase N Activatable Fluorescent Probe for Tracking Metastatic Cancer and Image-Guided Surgery via *in Situ* Spraying. *J. Am. Chem. Soc.* **2020**, *142*, 6381–6389, doi:10.1021/jacs.0c01365.
156. Hu, Z.; Fang, C.; Li, B.; Zhang, Z.; Cao, C.; Cai, M.; Su, S.; Sun, X.; Shi, X.; Li, C.; et al. First-in-Human Liver-Tumour Surgery Guided by Multispectral Fluorescence Imaging in the Visible and near-Infrared-I/II Windows. *Nat. Biomed. Eng.* **2019**, *4*, 259–271, doi:10.1038/s41551-019-0494-0.
157. Xu, J.; Yu, S.; Wang, X.; Qian, Y.; Wu, W.; Zhang, S.; Zheng, B.; Wei, G.; Gao, S.; Cao, Z.; et al. High Affinity of Chlorin E6 to Immunoglobulin G for Intraoperative Fluorescence Image-Guided Cancer Photodynamic and Checkpoint Blockade Therapy. *ACS Nano* **2019**, *13*, 10242–10260, doi:10.1021/acsnano.9b03466.
158. Lee, M.H.; Kim, J.Y.; Han, J.H.; Bhuniya, S.; Sessler, J.L.; Kang, C.; Kim, J.S. Direct Fluorescence Monitoring of the Delivery and Cellular Uptake of a Cancer-Targeted RGD Peptide-Appended Naphthalimide Theragnostic Prodrug. *J. Am. Chem. Soc.* **2012**, *134*, 12668–12674, doi:10.1021/ja303998y.
159. Xu, Z.; He, B.; Shen, J.; Yang, W.; Yin, M. Fluorescent Water-Soluble Perylenediimide-Cored Cationic Dendrimers: Synthesis, Optical Properties, and Cell Uptake. *Chem. Commun.* **2013**, *49*, 3646, doi:10.1039/c3cc40330k.
160. Cheng, W.; Cheng, H.; Wan, S.; Zhang, X.; Yin, M. Dual-Stimulus-Responsive Fluorescent Supramolecular Prodrug for Antitumor Drug Delivery. *Chem. Mater.* **2017**, *29*, 4218–4226, doi:10.1021/acs.chemmater.7b00047.
161. Cai, Y.; Ji, C.; Zhang, S.; Su, Z.; Yin, M. Synthesis of Water-Soluble Dye-Cored Poly(Amidoamine) Dendrimers for Long-Term Live Cell Imaging. *Sci. China Mater.* **2018**, *61*, 1475–1483, doi:10.1007/s40843-018-9246-6.
162. Maiti, S.; Park, N.; Han, J.H.; Jeon, H.M.; Lee, J.H.; Bhuniya, S.; Kang, C.; Kim, J.S. Gemcitabine–Coumarin–Biotin Conjugates: A Target Specific Theranostic Anticancer Prodrug. *J. Am. Chem. Soc.* **2013**, *135*, 4567–4572, doi:10.1021/ja401350x.
163. Bhuniya, S.; Maiti, S.; Kim, E.; Lee, H.; Sessler, J.L.; Hong, K.S.; Kim, J.S. An Activatable Theranostic for Targeted Cancer Therapy and Imaging. *Angew. Chem. Int. Ed.* **2014**, *53*, 4469–4474, doi:10.1002/anie.201311133.
164. Yang, Z.; Lee, J.H.; Jeon, H.M.; Han, J.H.; Park, N.; He, Y.; Lee, H.; Hong, K.S.; Kang, C.; Kim, J.S. Folate-Based Near-Infrared Fluorescent Theranostic Gemcitabine Delivery. *J. Am. Chem. Soc.* **2013**, *135*, 11657–11662, doi:10.1021/ja405372k.

 doi:10.20944/preprints202602.0438.v1

165. Xu, Z.; Guo, K.; Yu, J.; Sun, H.; Tang, J.; Shen, J.; Müllen, K.; Yang, W.; Yin, M. A Unique Perylene-Based DNA Intercalator: Localization in Cell Nuclei and Inhibition of Cancer Cells and Tumors. *Small* **2014**, *10*, 4087–4092, doi:10.1002/smll.201401262.
166. Xu, Z.; Cheng, W.; Guo, K.; Yu, J.; Shen, J.; Tang, J.; Yang, W.; Yin, M. Molecular Size, Shape, and Electric Charges: Essential for Perylene Bisimide-Based DNA Intercalator to Localize in Cell Nuclei and Inhibit Cancer Cell Growth. *ACS Appl. Mater. Interfaces* **2015**, *7*, 9784–9791, doi:10.1021/acsami.5b01665.